Article

Gli1/DNA interaction is a druggable target for Hedgehog-dependent tumors

Paola Infante[1,†], Mattia Mori[1,†], Romina Alfonsi[2,†], Francesca Ghirga[3], Federica Aiello[4], Sara Toscano[1], Cinzia Ingallina[1], Mariangela Siler[2], Danilo Cucchi[2], Agnese Po[2], Evelina Miele[1], Davide D'Amico[2], Gianluca Canettieri[2], Enrico De Smaele[5], Elisabetta Ferretti[5], Isabella Screpanti[2], Gloria Uccello Barretta[4], Maurizio Botta[6,7], Bruno Botta[3,***], Alberto Gulino[1,2,8,9,**] & Lucia Di Marcotullio[2,*]

Abstract

Hedgehog signaling is essential for tissue development and stemness, and its deregulation has been observed in many tumors. Aberrant activation of Hedgehog signaling is the result of genetic mutations of pathway components or other Smo-dependent or independent mechanisms, all triggering the downstream effector Gli1. For this reason, understanding the poorly elucidated mechanism of Gli1-mediated transcription allows to identify novel molecules blocking the pathway at a downstream level, representing a critical goal in tumor biology. Here, we clarify the structural requirements of the pathway effector Gli1 for binding to DNA and identify Glabrescione B as the first small molecule binding to Gli1 zinc finger and impairing Gli1 activity by interfering with its interaction with DNA. Remarkably, as a consequence of its robust inhibitory effect on Gli1 activity, Glabrescione B inhibited the growth of Hedgehog-dependent tumor cells *in vitro* and *in vivo* as well as the self-renewal ability and clonogenicity of tumor-derived stem cells. The identification of the structural requirements of Gli1/DNA interaction highlights their relevance for pharmacologic interference of Gli signaling.

Introduction

Inappropriate reactivation of the Hedgehog (Hh) developmental signaling pathway is responsible for the formation and progression of several human cancers through aberrant regulation of the functional properties of cancer stem cells (i.e. self-renewal, survival, metastatic spread, neoangiogenesis) (reviewed in Gulino *et al*, 2012; Amakye *et al*, 2013; Briscoe & Thèrond, 2013; Aberger & Ruiz I Altaba, 2014). Autocrine/paracrine Shh, Ihh or Dhh ligands bind to Patched (Ptch) receptor relieving its repressive activity on the seven-transmembrane protein Smoothened (Smo), which in turn activates the downstream transcription factors belonging to the Gli family. Gli proteins harbor a five zinc finger (ZF) region in which ZF4 and ZF5 domains bind target DNA in a sequence-specific way, whereas ZF1, ZF2 and ZF3 bind the phosphate backbone and possibly contributed to control binding stability and recruitment of co-regulatory factors (Kinzler & Vogelstein, 1990; Pavletich & Pabo, 1993). A C-terminal region is provided of transactivating function through modulation of chromatin remodeling induced by recruitment of TFIID TATA box-binding protein-associated factor TAFII31 (Yoon *et al*, 1998; Bosco-Clément *et al*, 2013) or HAT and HDAC (Canettieri *et al*, 2010; Malatesta *et al*, 2013), SWI-SNF5 (Jagani *et al*, 2010) and SWI/SNF-like Brg/Brm-associated factor (Zhan *et al*, 2011). In this way, Gli transcription factors behave as the final effectors for the control of specific oncogenic target genes (Aberger & Ruiz I Altaba, 2014). Although many Hh-driven human cancers involve upstream pathway activation (i.e. either loss-of-function Ptch1 or gain-of-function Smo

1 Center for Life NanoScience@Sapienza, Istituto Italiano di Tecnologia, Rome, Italy
2 Department of Molecular Medicine, University La Sapienza, Rome, Italy
3 Dipartimento di Chimica e Tecnologie del Farmaco, University La Sapienza, Rome, Italy
4 Department of Chemistry and Industrial Chemistry, University of Pisa, Pisa, Italy
5 Department of Experimental Medicine, University La Sapienza, Rome, Italy
6 Department of Biotechnology, Chemistry and Pharmacy, University of Siena, Siena, Italy
7 Sbarro Institute for Cancer Research and Molecular Medicine, Temple University, Philadelphia, PA, USA
8 Istituto Pasteur, Fondazione Cenci-Bolognetti - University La Sapienza, Rome, Italy
9 IRCCS Neuromed, Pozzilli, Italy
*Corresponding author. Tel: +39 649255657; Fax: +39 649255660; E-mail: lucia.dimarcotullio@uniroma1.it or
**Corresponding author. Tel: +39 649255129; Fax: +39 649255660; E-mail: alberto.gulino@uniroma1.it or
***Corresponding author. Tel: +39 649912781; E-mail: bruno.botta@uniroma1.it
†These authors contributed equally to this work

mutations or Smo activation by loss of cAMP/PKA-mediated inhibitory Gα-GNAS tumor suppressor or ligand overproduction) (Goodrich et al, 1997; Yauch et al, 2009; He et al, 2014), several tumors harbor Smo-independent increased function of the downstream Gli effectors, due to high protein levels or activatory mechanisms (i.e. Gli gene amplification or epigenetically driven overexpression, mutation in or loss of heterozygosity of SuFu gene or a number of post-synthetic modifications such as decreased ubiquitination-mediated degradation or acetylation of the Gli proteins or increased PI3K/mTOR/S6K1 kinase-dependent phosphorylation) (Kinzler et al, 1987; Taylor et al, 2002; Dahlén et al, 2004; Di Marcotullio et al, 2006a, 2011; Canettieri et al, 2010; Wang et al, 2012; Mazzà et al, 2013; Tang et al, 2014). Notwithstanding, the mechanisms of regulation of Gli functions and the way it interacts with target DNA and controls transcription are still poorly understood.

Small molecules have been reported to represent helpful tools to understand the mechanisms of modulation of Hh/Gli function at the level of Smo transducer and Gli effector. This allowed the development of several inhibitors targeting components of the pathway in order to control tumor growth. However, whereas several Smo antagonists are currently investigated in clinical trials (GDC-0449 has been recently approved by FDA), a few Gli inhibitors have been identified (Mas & Ruiz I Altaba, 2010; Coni et al, 2013a). Therefore, novel drugs targeting specific molecular steps underlying Gli function would be beneficial either for a wide spectrum of patients whose tumors have high Gli protein levels and/or activity. Furthermore, downstream activation of Gli function is frequently occurring with the appearance of resistance to Smo antagonists observed during therapy (Galimberti et al, 2012; Amakye et al, 2013). The lack of information on the structural and functional requirements of Gli1/DNA interaction accounts for the low number of small molecules inhibiting Gli. HPI-1 and HPI-4 have been shown to target the post-translational events of Gli processing/activation downstream of Smo, such as increase of the proteolytic cleavage of Gli2-FL to its repressor form Gli2-R or overall Gli1 degradation (Hyman et al, 2009). Arsenic trioxide (ATO) has been recently shown to prevent Gli2 localization to primary cilium, thus leading to its proteolytic degradation, while binding-dependent inactivation of Gli1 has not been yet characterized (Kim et al, 2010; Beauchamp et al, 2011). Similarly, GANT61 inhibits Gli1/DNA binding only in living cells, suggesting that it indirectly impairs its interaction with target gene promoters by as yet unelucidated mechanisms (Lauth et al, 2007).

Based on the knowledge of the crystallographic structure of the zinc finger domain of Gli1 (Gli1ZF) in complex with DNA (Pavletich & Pabo, 1993), together with NMR studies as well as computational and experimental mutagenesis, we clarify here the structural requirements of Gli1/DNA interaction and identify Glabrescione B (GlaB), an isoflavone naturally found in the seeds of Derris glabrescens (Leguminosae), as a novel small molecule that binds Gli1ZF and interferes with its interaction with DNA. This small molecule turned out to be an efficient inhibitor of the growth of Hh/Gli-dependent tumors and cancer stem cells in vitro and in vivo, indicating that Gli/DNA interference is an appealing therapeutic strategy to control the heterogeneous molecular changes leading to Hh/Gli pathway activation in cancer.

Results

Structural and functional requirements for Gli1/DNA interaction

To identify the molecular bases of the function of the Gli1/DNA complex, we established a computational screening protocol, based on the available X-ray structure of cobalt ion-coordinated Gli1ZF in complex with DNA (Pavletich & Pabo, 1993) that, although structurally relevant, does not provide by itself information on the energy of the system. Therefore, we investigated the conformational dynamics using the physiological zinc within the Zn-coordination system of each zinc finger by performing four independent replicas of molecular dynamics (MD) simulations. A representative Gli1ZF structure was extracted from MD trajectories (Fig 1A, Supplementary Movie S1) for further ligand design in silico.

Based on MD analysis and X-ray structure, the impact of serine and basic residues of ZF4 and ZF5 on the thermodynamic stability of the Gli1ZF/DNA adduct was evaluated by computational alanine scanning. The delta energy (ΔG) of binding of Gli1 mutants to DNA was calculated along MD trajectories (Fig 1B, Supplementary Table S1) and compared to the wild-type Gli1ZF (Gli1ZF-WT) ($\Delta\Delta G$). The results show that the strongest $\Delta\Delta G$ contribution was given by basic residues involved in H-bonding DNA bases or in electrostatic interaction with the phosphate backbone of DNA. Indeed, mutation in silico of K340, K350, R354 in ZF4 and K360, K371, R380 and K381 of ZF5 strongly impaired the Gli1ZF ΔG of binding to DNA.

To correlate these observations with transactivating function of Gli1, we performed a functional assay in HEK293T cells, transiently expressing ectopic Gli1 or different Gli1ZF mutants and a Gli-dependent luciferase reporter driven by a Gli-responsive consensus sequence. Mutations in K350 and R354 in ZF4 or R380 and K381 in ZF5 completely abrogated the transcriptional activity of Gli1, whereas K340, K371 and K360 did it to a lesser extent. Notably, a significant linear correlation was obtained ($R^2 = 0.6918$) by comparing each theoretical $\Delta\Delta G$ value with the respective percentage of luciferase activity observed in cell assays.

Mutagenesis studies suggested that the above residues may be involved in Gli1 binding to DNA (Fig 1C, Supplementary Table S1). We chose the K350A and K340A mutants, showing the highest and intermediate $\Delta\Delta G$ of binding, respectively (Supplementary Table S1), to test their direct interaction with DNA. An electrophoretic mobility shift assay (EMSA) was performed using equal amounts of recombinant GST-Gli1ZF-WT or GST-Gli1ZF-K350A or GST-Gli1ZF-K340A (Supplementary Fig S2) and a DNA probe containing Gli-responsive consensus DNA sequence or a mutated version unable to bind Gli1 (Fig 1D and E). Comparison with the strong DNA binding affinity of the recombinant GST-Gli1ZF-WT confirms that GST-Gli1ZF-K350A was unable to bind DNA, whereas GST-Gli1ZF-K340A did it, albeit to a significantly lower extent (Fig 1E, Supplementary Fig S2). Notably, these results correlate with the impaired and intermediate transcriptional activity of Gli1ZF-K350A and Gli1ZF-K340A mutants in cell-based assays, respectively (Fig 1C), and suggest that both K350 and K340 are involved in DNA binding and transcriptional activity, although with a different strength.
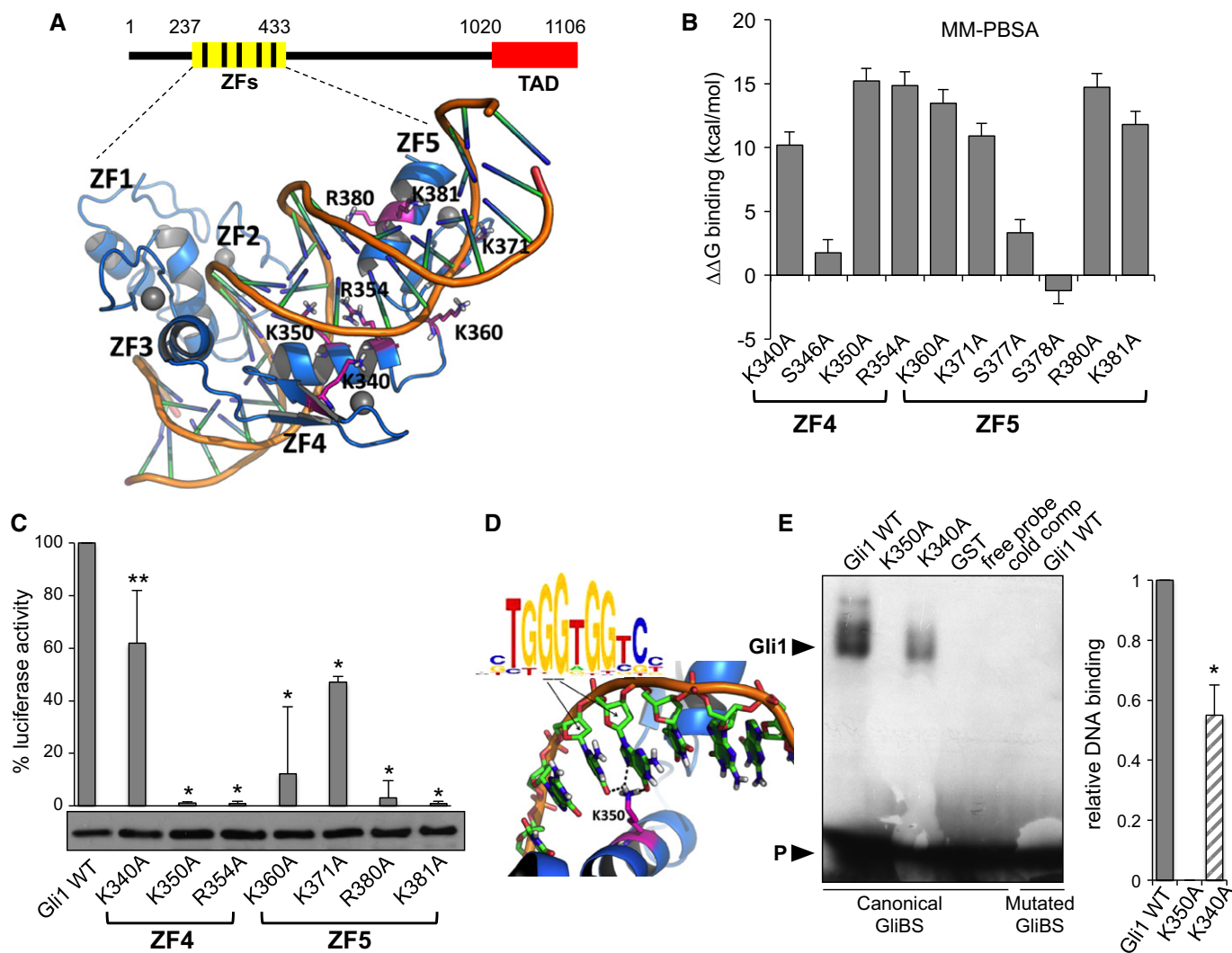
Figure 1. Structure-based analysis of Gli1/DNA complex.

A   Representative Gli1ZF/DNA structure extrapolated from MD trajectories. Gli1ZF is shown as blue cartoon, residues involved in binding to DNA (based on single point mutation study) are shown as magenta sticks, and Zn ions as gray spheres.

B   Effect of Gli1ZF mutants on the binding affinity to DNA as predicted by *in silico* alanine scanning. The ΔΔG was calculated along MD trajectories as the difference between the ΔG of each Gli1ZF alanine mutant and Gli1ZF-WT. Results are shown as ΔΔG values in kcal/mol calculated by means of the MM-PBSA methods ± SEM.

C   Effect of Gli1ZF mutants on Gli1-dependent transcriptional activation. Luciferase assay was performed in HEK293T cells transfected with 12XGliBS-Luc (GliBS, Gli binding site), pRL-TK *Renilla* (normalization control), Flag-Gli1 WT or the indicated Flag-Gli1 mutants. Data show the mean ± SD of three independent experiments. *$P < 0.01$; **$P < 0.05$ versus Gli1 WT. Western blot analysis of Flag-Gli1 WT or the indicated Flag-Gli1 mutant expression levels (bottom panel).

D   Specific H-bond interactions between K350 of Gli1ZF and Gli1 binding site consensus, as predicted by MD.

E   Gli1/DNA binding. Double-stranded oligonucleotide containing the canonical GliBS sequence (5′–TTGCCTACCTGGGTGGTCTCTCCACTT–3′) or mutated GliBS sequence used as control (5′–TTGCCTACCTCCCACTTCTCTCCACTT–3′) was used as probe (P) in EMSA experiments. The assay was performed using recombinant GST-Gli1ZF-WT (Gli1 zinc finger fragment: aa 242–424), GST-Gli1ZF-K350A and GST-Gli1ZF-K340A. The graph on the right indicates ratio (mean arbitrary units ± SD from three independent experiments) of GST-Gli1ZF-WT or GST-Gli1ZF mutants bound to the labeled GliBS probe/GliBS-free probe normalized to the amount of GST-Gli1ZF-WT/DNA binding (as described in Materials and Methods). *$P < 0.05$ versus Gli1 WT.

Source data are available online for this figure.

Virtual library and transcriptional screening of Gli1 interacting small molecules

To understand whether Gli1 binding to DNA and function could be regulated by small molecules, an in house library composed of more than 800 unique natural compounds was docked toward the MD representative Gli1ZF structure using the GOLD program (Supplementary Fig S3) (Verdonk *et al*, 2003). Literature data (Sheng *et al*, 2006) and results of the mutagenesis study were used to set up docking and analyze ligand poses, respectively. Indeed, only small molecules able to interact at least with one of the basic residues highlighted by the mutagenesis study were selected. The ligand ΔG

of binding was then computed by means of the MM-GBSA method (Mori *et al*, 2011) and divided by the number of heavy atoms to provide the ligand efficiency (LE) as the final scoring parameter. We identified six molecules (three vismiones, GlaB, the chalcone V94 and the opioid alkaloid narceine) putatively behaving as potential Gli1 inhibitors (Supplementary Fig S4A). To investigate the functional activity of these compounds as specific modulators of Gli1, we used the Gli-dependent luciferase reporter screening assay. Whereas GlaB and Vismione E inhibited luciferase activity to a similar extent as GANT61 (a previously characterized Gli1 antagonist, Lauth *et al*, 2007), Vismione B only partially displayed inhibitory activity and other compounds were not active at all in this context (Fig 2A, Supplementary Fig S4B and C). Since vismiones have been shown to be quite chemically unstable in different conditions (Delle Monache, 1985), thus possibly limiting the identification of the bioactive specie, we focused further studies only on GlaB (Fig 2B).

Structural requirements for Gli1/GlaB interaction

To investigate whether the Gli1 inhibitory activity of GlaB was associated to the direct interaction of this small molecule with the transcription factor, we monitored by NMR spectroscopy the GlaB proton mono-selective relaxation rates (R^{ms}), which prove the slowing down of the small molecule motion upon binding to a receptor (Valensin *et al*, 1986; Neuhaus & Williamson, 1989). To this end, the protons H-1 and H-3 and the C-2 and C-4 methoxyl groups were chosen as probe for the interaction of ring A, proton H-11, H-12 and H-15 for ring B and proton H-8 for ring C (Table 1; Fig 2B).

First, mono-selective relaxation rates of free GlaB (R_f) were measured to normalize the R^{ms} detected in GlaB/protein mixtures (Table 1). In the presence of GST-Gli1ZF, a significant increase in R^{ms} was observed for the vicinal protons H-11 and H-12 (ring B), and to a lesser extent H-15 (ring B) and H-8 (ring C) (Table 1; Supplementary Fig S5). Instead, the R^{ms} of ring A protons were not perturbed by the presence of GST-Gli1ZF-WT and very likely were not involved in binding to Gli1ZF. To rule out any possible interference by the sole recombinant GST, we also monitored the R^{ms} of GlaB in the GlaB/GST mixture, showing a weak and unspecific involvement of all rings A, B and C (Table 1; Supplementary Fig S5). Therefore, ring B was identified as the specific molecular determinant for the interaction between GlaB and GST-Gli1ZF.

Although NMR analysis of O-prenyl groups was not too informative, because of the broad proton signals, they might be crucial for the correct positioning of GlaB ring B. Indeed, molecular docking studies showed that GlaB and Vismione B and E preferably bind within the same site at the interface between ZF4 and ZF5, with a noticeable shape and pharmacophoric overlapping (Supplementary Fig S6). The O-prenyl group at C-13 of GlaB is clearly overimposed to that of Vismione E, suggesting that a prenyl chain in this position may be relevant for Gli1 inhibition. GlaB derivatives without prenyl chains (Supplementary Fig S7) were also tested through the Gli-dependent luciferase reporter assay, but none of them was active, reinforcing that ring B prenyl chains may be important for GlaB biological activity.

To investigate the role of Gli1 K340 and K350 residues, both involved in DNA binding and transcriptional function (Fig 1C–E),

we monitored R^{ms} of GlaB with the GST-Gli1ZF-K340A single mutant or the GST-Gli1ZF-K340A/K350A double mutant. Notably, the specific interaction of GlaB ring B was preserved in binding to the Gli1ZF-K340A, although with weaker local affinity (Table 1; Supplementary Fig S5). This suggests that GlaB may adopt a similar binding conformation toward Gli1ZF-WT and Gli1ZF-K340A. In contrast, the additional K350A mutation in the Gli1ZF-K340A/K350A double mutant completely affects the capability of GlaB ring B to interact with Gli1ZF, thus providing a GlaB proton pattern spanning non-specifically throughout rings A, B and C, as observed with the sole GST (Table 1, Supplementary Fig S5).

In summary, results of NMR studies show that GlaB interacts directly with Gli1 and further emphasize the role of K340 and K350. The ring B and prenyl groups turned out to be key determinants for GlaB activity.

GlaB inhibits Hh signaling by imparing Gli1/DNA binding and transcriptional activity

Confirming the ability of GlaB to target Gli1, this compound significantly inhibited the luciferase activity driven by a Gli-responsive element reporter in Smo$^{-/-}$ MEF cells transfected with ectopic Gli1 (Fig 2C). Consistently, GlaB reduced the expression of several endogenous Gli target genes, whereas unrelated transcripts were unaffected (Fig 2D and F), without influencing cell survival (Supplementary Fig S8). Indeed, GlaB suppressed Hh gene signature in genetically defined Ptch1$^{-/-}$ mouse embryonic fibroblasts (Ptch1$^{-/-}$ MEFs) (Fig 2D), in which deletion of the inhibitory Ptch1 receptor releases Smo function and leads to a constitutive activation of Gli transcription factors (Goodrich *et al*, 1997) (Fig 2E). To further prove that GlaB is acting downstream of Smo, we used SuFu$^{-/-}$ MEFs. Reporter activity in these cells is high even in the absence of Shh or Smo stimulation, because of the loss of the well-known Gli1 inhibitor SuFu (Fig 2E), and is not suppressed by treatment with the Smo inhibitor cyclopamine (Svard *et al*, 2006). In this cellular context, GlaB reduced constitutive endogenous Hh target gene expression (Fig 2F). Moreover, ChIP assay in Gli1-overexpressing MEF cells showed a significant reduction of the recruitment of Gli1 into the promoter of Ptch1 gene (Fig 2G).

According to the high homology degree between ZF domain of Gli1 and Gli2, GlaB also inhibited Gli2-mediated transcription (Supplementary Fig S9). Conversely, since Jun/AP-1 has been reported to synergize with Gli1 while co-occupying the promoter region (Laner-Plamberger *et al*, 2009; Schnidar *et al*, 2009), we tested GlaB activity on this transcription factor. GlaB did not affect Jun/AP-1 activity (Supplementary Fig S10), further indicating its selectivity for Hh/Gli signaling. To better address the direct effect of GlaB on Gli, we knocked down Gli1 and Gli2 by siRNA (Fig 2H) in Hh-dependent Daoy tumor cells belonging to the Shh MB subgroup (Northcott *et al*, 2012; Triscott *et al*, 2013). GlaB was unable to repress Ptch1 mRNA levels in siGli1/Gli2-knocked down Daoy cells, indicating that the presence of Gli factors is required for GlaB activity.

Furthermore, *in vitro* enzymatic assays demonstrated that GlaB did not affect the catalytic activity of a number of protein kinases known to modulate Gli function (Supplementary Fig S11).
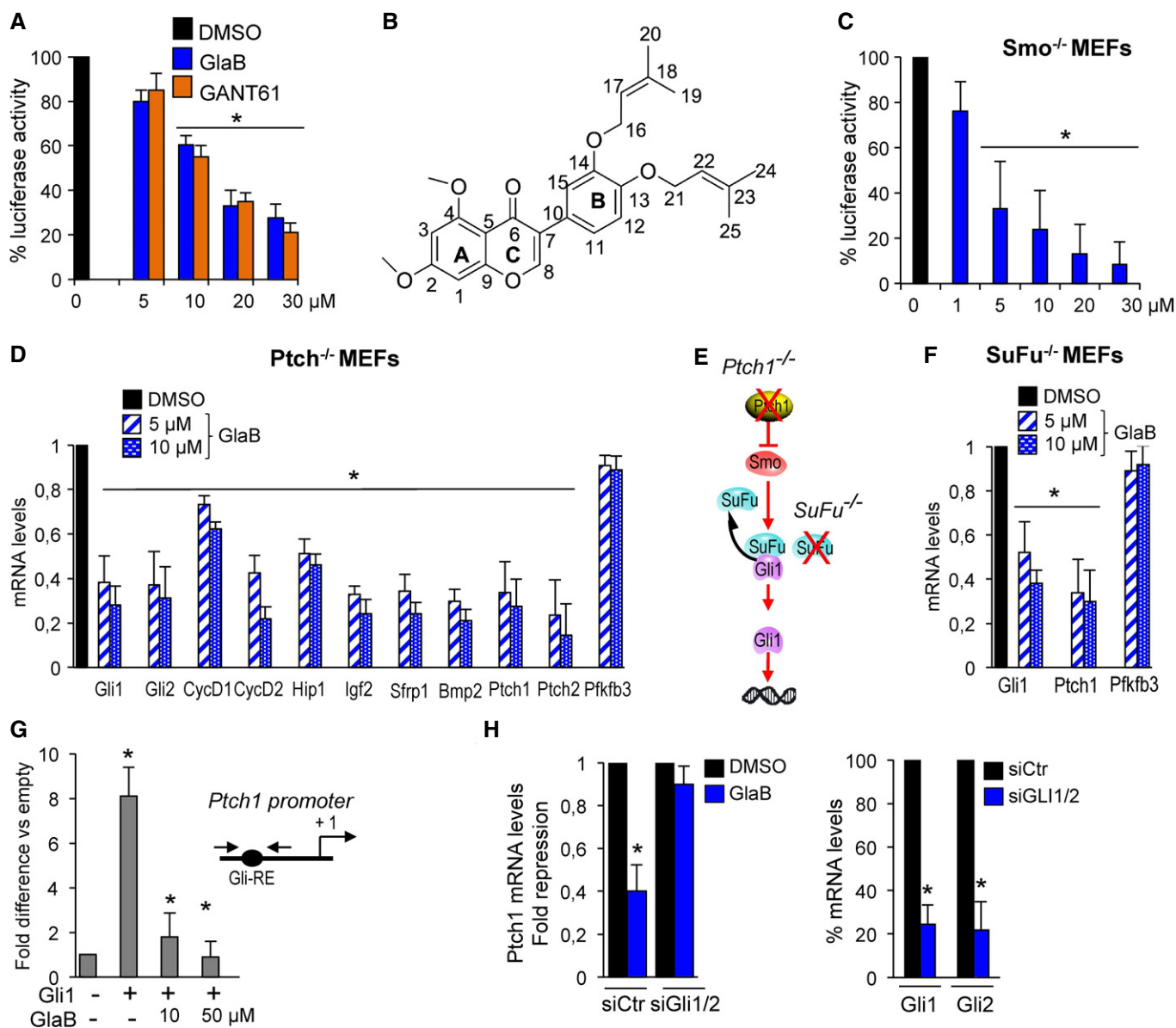
Figure 2.   GlaB inhibits Hh signaling by impairing Gli1 function.

A   Inhibition of Gli1-induced transcription in transfected HEK293T cells. HEK293T cells were transfected with 12XGliBS-Luc and pRL-TK *Renilla* (normalization control) plus control (empty) or Gli1 vector and treated with increasing concentrations of GlaB or GANT61. Treatment time was 24 h, and control cells were treated with DMSO only.

B   GlaB chemical structure with numbering scheme for NMR analysis.

C   Inhibition of Gli1-induced transcription in transfected Smo$^{-/-}$ MEF cells. Smo$^{-/-}$ MEF cells were transfected with 12XGliBS-Luc and pRL-TK *Renilla* (normalization control) plus control (empty) or Gli1 vector and treated for 24 h with increasing concentrations of GlaB or DMSO only as control.

D   The graphs show the Hh target gene expression levels in Ptch1$^{-/-}$ MEFs treated for 48 h with GlaB and DMSO as a control. mRNA levels were determined by quantitative real-time PCR (qRT–PCR) normalized to endogenous control (β2-microglobulin and *HPRT*). *Pfkfb3* gene was used as a negative control.

E   Representative model of Hh signaling hyperactivation: in Ptch1$^{-/-}$ MEFs, constitutive activation of Smo and consequently of Gli1; in SuFu$^{-/-}$ MEFs, release of Gli1 suppression.

F   SuFu$^{-/-}$ MEFs were treated for 48 h with GlaB and DMSO as a control. *Gli1* and *Ptch1* mRNA levels were determined by qRT–PCR normalized to β2-microglobulin and *HPRT* expression. *Pfkfb3* gene was used as a negative control.

G   Promoter occupancy of Gli1 is prevented by GlaB treatment. MEF WT cells were transfected with Flag-tagged Gli1 or empty vectors, and chromatin immunoprecipitation (ChIP) was carried out. qRT–PCR was performed using primers encompassing the Gli-BS of mouse *Ptch1* promoter (right, schematic representation). Results are indicated as fold difference, relative to empty (pcDNA3) control.

H   *Ptch1* mRNA expression levels (left panel) were determined by qRT–PCR in Daoy cells transfected with siRNA specific for Gli1 and Gli2 (siGli1/2) or a non-specific control siRNA (siCtr) and treated for 24 h with GlaB or DMSO as a control. (right panel) The graph shows *Gli1* and *Gli2* mRNA expression levels determined by qRT–PCR in Daoy cells transfected with siGli1/2 or siCtr. Results are expressed as fold repression relative to control, and data were normalized to *GAPDH* and *HPRT* expression.

Data information: All data show the mean ± SD of three independent experiments. *P < 0.05 versus DMSO.

Table 1. Monoselective relaxation rates (R^{ms}, s^{-1}) of selected protons of GlaB (0.412 mM, 600 MHz, DMSO-d_6, 25°C) and corresponding values of normalized relaxation rates ($\Delta R/R_f$, where $\Delta R = R^{ms}$-R_f) in different mixtures.

Proton	RING	$R_f(s^{-1})$	GlaB/GST-Gli1ZF $\Delta R/R_f$	GlaB/GST-Gli1ZF K340A $\Delta R/R_f$	GlaB/GST-Gli1ZF K340A/K350A $\Delta R/R_f$	GlaB/GST $\Delta R/R_f$
H-1	A	0.41	0	0	0.03	0.02
2-OMe	A	1.20	0	0	0.05	0.06
H-3	A	0.63	0	0	0.05	0.10
4-OMe	A	1.39	0	0	n.d.[a]	0
H-8	C	0.36	0.13	0.05	0.07	0
H-11	B	0.63	1.20	0.15	0.38	0.22
H-12	B	0.89	0.95	0.23	n.d.[b]	0.03
H-15	B	0.76	0.22	0.22	0.14	0.14

[a]Relaxation rate of 4-OMe protons was not determined because its signal was partially superimposed to that of the water.
[b]Relaxation rate of proton H-12 was not measured because of the large linewidth.

Analysis of GlaB binding mode to Gli1

The possible binding mode of GlaB to the representative Gli1 structure extrapolated from MD was investigated by molecular docking. Although Gli1 is characterized by a scarce druggability, mostly due to a rather flat surface, a high flexibility and the lack of deep lipophilic pockets, a significant cluster of top-ranking poses was found in a surface groove between ZF4 and ZF5 (Fig 3A, Supplementary Fig S12). The putative GlaB binding site was bounded by the residues at the N-terminal of ZF5 helix and by the side chain of K340, which significantly contributes to sculpt the groove over the side chain of R354 where the GlaB ring B performed its most profitable interactions, in good agreement with NMR data (Fig 3B, Supplementary Figs S5 and S12). Besides non-specific hydrophobic contacts within the putative binding site, GlaB also performed H-bond interaction with the side chain of K350, a key residue in determining Gli1/DNA binding and Gli1 transcriptional function (Fig 1B–E).

Moreover, the binding of GlaB to Gli1ZF-K340A, Gli1ZF-K350A and Gli1ZF-K340A/K350A mutants was also investigated by molecular modeling and compared to that observed toward Gli1ZF-WT. In agreement with NMR data, K350 was highlighted as the major anchor point for GlaB within Gli1ZF. Indeed, in Gli1ZF-WT and the Gli1ZF-K340A mutant, GlaB adopted a very similar binding conformation and contacted K350 by H-bond interactions (Fig 3B). Mutation of K350 to alanine significantly affected the specificity of GlaB binding, as the small molecule was no more able to interact within ZF4 and ZF5 (Fig 3B). Prediction of the ΔG of binding and pK_d values showed that GlaB has the highest affinity for Gli1ZF-WT, whereas its affinity for Gli1ZF-K340A was slightly lower (Fig 3B), in agreement with NMR studies and biological results. Contrarily, the predicted GlaB affinity for Gli1ZF-K350A and Gli1ZF-K340A/K350A was significantly lower than for Gli1ZF (Fig 3B), thus reinforcing the structural relevance of K350 for Gli1 function and inhibition.

Therefore, we hypothesized that, by interacting with Gli1, GlaB might impair its interaction with target DNA. As verified by EMSA, the formation of Gli1ZF-WT/consensus DNA complex was strongly prevented by GlaB (Fig 3C). The formation of DNA/Gli1ZF-K340A single mutant is partially impaired with respect to WT protein, implying a role of K340 in strengthening the binding with DNA.

However, the complex was still targeted by GlaB (Fig 3C), suggesting its activity on the residual K350 amino acid of Gli1.

Consistent with the involvement of both K340 and K350 in interaction with GlaB, this small molecule partially inhibited both the formation of the DNA/Gli1ZF-K340A complex (Fig 3C) and the transacting activity of the Gli1-K340A mutant compared to Gli1 WT (Fig 3D), thus suggesting that GlaB binding to K340 contributes to Gli1 inhibition.

Overall, these findings strongly support a GlaB direct inhibitory activity on Gli1 by interfering with the cooperation of both K340 and K350 for binding to DNA and transcription function, thus blunting Gli-driven gene expression.

GlaB inhibits Gli-dependent growth of cerebellum-derived normal progenitors *in vitro* and *in vivo*

Subversion of Hh-dependent development of cerebellum is critical for medulloblastoma (MB) formation (Wechsler-Reya & Scott, 2001; Hatten & Roussel, 2011). Indeed, Hh signaling is crucial for enhancing the expansion of a subset of granule cell progenitors (GCPs) that populate the external germinal layer (EGL) of the cerebellar cortex during the first week after birth in mice (Di Marcotullio *et al*, 2006b). This process is triggered by Purkinje cell-derived Shh and is required for intense GCP proliferation and proper development of the granule neuron lineage. Importantly, the lack of GCP proliferation arrest caused by withdrawal of Hh signal, which physiologically occurs after the first week of age, is responsible for the tumorigenic conversion of these progenitors, considered as the cell of origin of MB (Schuller *et al*, 2008; Yang *et al*, 2008). In fact, mice harboring either loss-of-function Ptch1 or gain-of-function Smo mutations develop MB where Gli-dependent activation of specific oncogenic programs (i.e. NMyc, IGF2) is required for tumor formation (Hahn *et al*, 2000; Roussel & Robinson, 2013). Similar defects of Hh signaling pathway are responsible for human MB (Goodrich *et al*, 1997).

To assess the *in vivo* efficacy of GlaB to interfere with Hh-dependent growth events, we first tested its ability to suppress Hh signaling in 6-day-old mouse cerebellar progenitors. GlaB treatment reduced significantly the levels of several Gli target genes in the cerebellar tissue *in vivo* (i.e. Gli1, Gli2, Ptch, Hip1) including genes
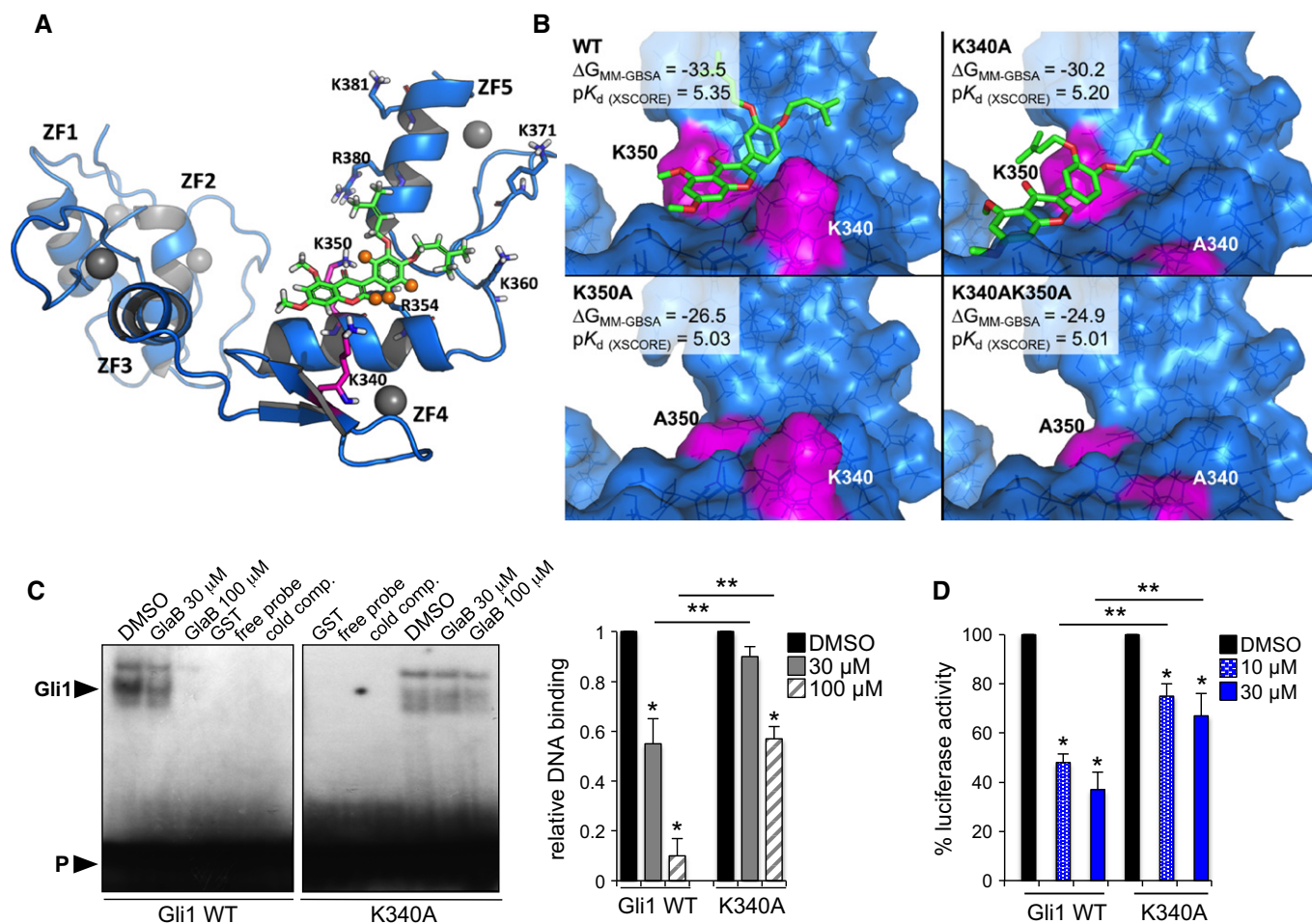
Figure 3. Analysis of Gli1/GlaB interaction.

A   The predicted binding mode of GlaB (green sticks) to Gli1ZF (blue cartoons). Residues highlighted by the single-point mutation study to impact on Gli1 binding to DNA are shown as blue sticks; K340 and K350 of the GlaB binding site are colored magenta. GlaB protons highlighted by the NMR study are shown as orange spheres.

B   Detail of GlaB binding to Gli1ZF-WT, Gli1ZF-K340A, GLI1ZF-K350A, GLI1ZF-K340A/K350A mutants and respective theoretical affinity values. Gli1 is shown as blue transparent surface; K340 and K350 are colored magenta. GlaB is shown as green sticks.

C   Inhibition of Gli1/DNA binding by GlaB. EMSA using recombinant GST-Gli1ZF-WT or GST-Gli1ZF-K340A in the presence of different concentrations of GlaB or with DMSO only. The shifted complex is competed with a 50× excess of cold probe. The graph on the right indicates ratio (mean arbitrary units ± SD from three independent experiments) of GST-Gli1ZF-WT or GST-Gli1ZF-K340A bound to the labeled GliBS probe/GliBS-free probe normalized to the amount of GST-Gli1ZF-WT/ DNA binding in absence of GlaB. *$P < 0.05$ versus DMSO; **$P < 0.05$ K340A + GlaB versus Gli1 WT + GlaB.

D   HEK293T cells were transfected with 12XGliBS-Luc and pRL-TK *Renilla* (normalization control) plus control (empty vector) or Gli1 or Gli1K340A mutant and treated with increasing concentrations of GlaB. Treatment time was 24 h, and control cells were treated with DMSO only. Data show the mean ± SD of three independent experiments. *$P < 0.05$ versus DMSO; **$P < 0.05$ K340A versus Gli1 WT.

Source data are available online for this figure.

directly involved in Hh-dependent cell proliferation (cyclins D1 and D2, NMyc, IGF2) (Fig 4A). A significant inhibition of GCPs proliferation *in vivo* was observed in response to GlaB treatment, since the thickness of EGL and the Ki67-labeled cell immunostaining were reduced (Fig 4B and C). These data confirmed the *in vitro* ability of GlaB to downregulate the Shh-enhanced BrdU uptake of cultured GCPs isolated from 4-day-old mice cerebella in a dose-dependent way (Fig 4D). Consistently, GCPs isolated from mice treated *in vivo* with GlaB displayed reduced levels of mRNA and protein of several Hh target genes and markers related to cell proliferation (i.e. Gli1, Gli2, HIP1, Ptch, PCNA, cyclins D1 and D2, NMyc, IGF2) (Fig 4E and F).

GlaB inhibits the growth of Gli-dependent medulloblastoma and tumor-derived stem-like cells

To verify the GlaB efficacy to inhibit Hh-dependent MB cell growth, primary MB cells were freshly isolated from Ptch1^{+/−} mice tumors and tested in short-term cultures to keep Hh sensitivity *in vitro* (Berman *et al*, 2002; Sasai *et al*, 2006; Kool *et al*, 2014). As shown in Fig 5A, GlaB significantly inhibited the proliferation of Ptch1^{+/−} MB cells with a strength similar to GANT61. Moreover, GlaB also induced a striking decrease of Gli1 mRNA levels (Fig 5B). Notably, no effect was observed in Hh-independent HepG2 hepatocellular
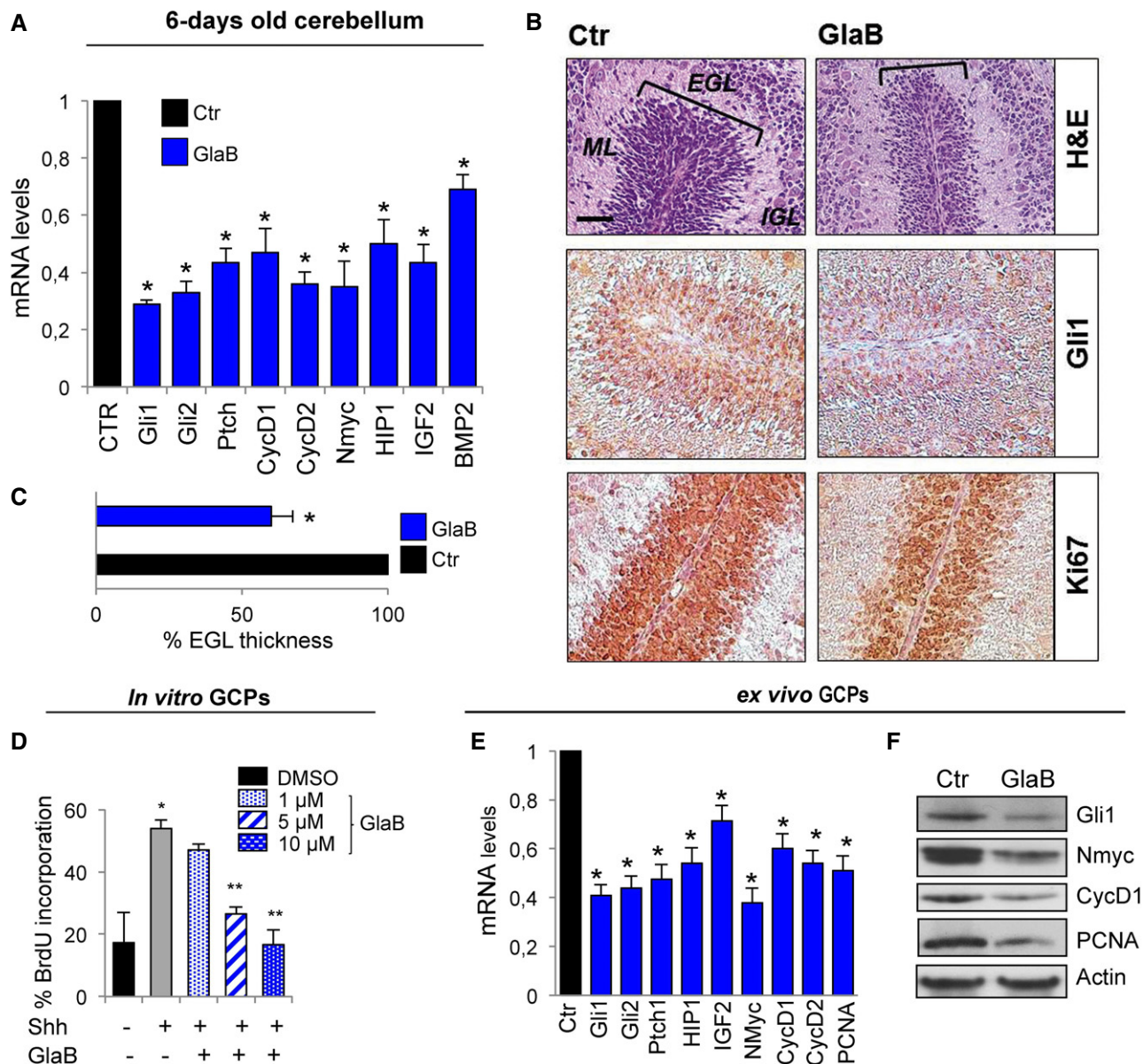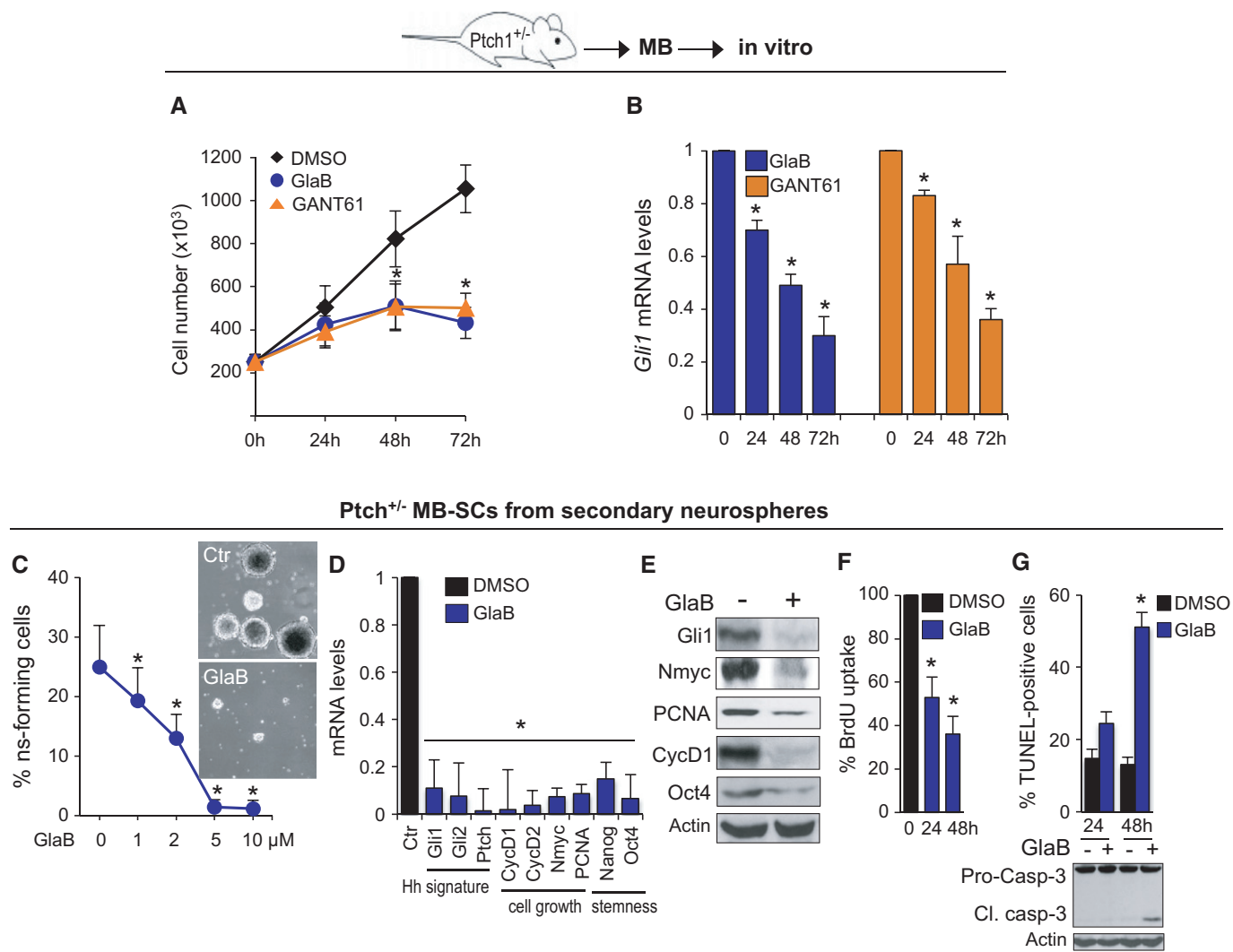
Figure 4. GlaB inhibits Gli1-dependent growth of cerebellum-derived normal progenitors.

A   qRT–PCR shows Hh target mRNA expression levels determined in 6-day-old mouse cerebellar progenitors after s.c. injections of GlaB.

B   Representative EGL H&E staining of 6-day-old mouse cerebellum after s.c. injections of GlaB (upper panel); immunohistochemistry shows Gli1 (middle panel) and Ki67 stainings (lower panel). In all images, the scale bar represents 50 μm.

C   The graph shows the percentage of EGL thickness reduction in GlaB-treated mouse cerebella in comparison with vehicle mouse cerebella. Data show the mean ± SD of cerebella ($n = 10$) for each treatment. *$P < 0.05$ versus Ctr.

D   BrdU assay in GCPs. Cerebellar granule cell progenitors (GCPs) isolated from 4-day-old mice were treated with Shh (recombinant mouse Sonic Hedgehog, amino-terminal peptide, ShhN, 3 μg/ml) and with different concentrations of GlaB, as indicated, for 48 h. Inhibition of cell proliferation was measured as percentage of BrdU incorporation in comparison with DMSO-treated sample. Shown is the mean of three independent experiments. Error bars indicate SD. *$P < 0.05$ Shh versus DMSO; **$P < 0.05$ Shh + GlaB versus Shh.

E, F   qRT–PCR and Western blot analysis show Hh and proliferation target mRNA and protein expression levels determined in *ex vivo* GCP culture derived from 6-day-old mouse cerebella after s.c. injections of GlaB. In all qRT–PCR experiments, the results were normalized to endogenous control (β2-microglobulin and *HPRT*). *$P < 0.05$ versus Ctr.

Source data are available online for this figure.

carcinoma cells or Jurkat T leukemia cells, which display undetectable levels of Gli1 (Lauth *et al*, 2007; Beauchamp *et al*, 2011) (Supplementary Fig S13).

Several tumors, including MB, contain a small subset of stem-like cells (SCs) responsible for cancer cell population expansion (through unlimited self-renewal) that triggers tumorigenesis, drives

Figure 5.   Inhibition of Gli-dependent MB tumor cell growth.

A, B   *Ex vivo* cell cultures from Ptch1$^{+/-}$ mice MBs were treated with GlaB (5 μM), GANT61 (10 μM) or DMSO only. After the indicated times, a trypan blue count was performed (A) to determine the growth rate of viable cells. *Gli1* mRNA expression levels were determined by qRT–PCR (B) normalized to endogenous control (β2-microglobulin and *HPRT*).

C–F   GlaB inhibits MB-SCs' self-renewal and proliferation. (C) Suspension of single MB-SCs isolated from Ptch1$^{+/-}$ mice. MBs were cultured in stem cell medium to allow the formation of primary neurospheres. Primary neurospheres were dissociated and treated with increasing concentrations of GlaB or DMSO only. After 7 days of treatment, the number of secondary neurospheres derived from a known number of single cells was counted. The self-renewal MB-SCs' capability is expressed as percentage of neurosphere-forming cells (left). Representative bright field images of tumor neurospheres after GlaB treatment are also shown (right). (D, E) MB-SCs isolated from Ptch1$^{+/-}$ mice MBs were treated for 48 h with GlaB (5 μM) or DMSO only. qRT–PCR and Western blot analysis show Hh, proliferation and stemness target mRNA and protein expression levels. For qRT–PCR, results were normalized to endogenous control (β2-microglobulin and *HPRT*). (F) BrdU assay in MB-SCs treated with GlaB (5 μM) for 24 or 48 h and plated on polylysinated chamber slides. Inhibition of cell proliferation was measured as percentage of BrdU incorporation in comparison with DMSO-treated sample.

G   TUNEL assay in MB-SCs. MB-SCs isolated from Ptch1$^{+/-}$ mice MBs were treated with GlaB (5 μM) and compared to DMSO-treated sample. Bottom panel shows a Western blot of caspase-3 in GlaB-treated versus control cells.

Data information: In all experiments, data show the mean ± SD of three independent experiments. *$P < 0.05$ versus DMSO.
Source data are available online for this figure.

resistance to conventional therapies and favors tumor relapse (Manoranjan *et al*, 2013). Hh signaling pathway is crucial for the generation and maintenance of MB-SCs in human and mouse through Gli-mediated transcriptional activation of the Nanog stemness gene (Clement *et al*, 2007; Po *et al*, 2010; Garg *et al*, 2013), thus favoring tumorigenesis and MB progression. MB-SCs are therefore appealing candidates for testing the therapeutic potential

of the novel Gli inhibitor we have identified, in order to eradicate the tumor. We show that GlaB suppressed the ability of Ptch1$^{+/-}$ MB-SCs to form spheres from single cell suspension (an expression of their clonogenic self-renewal ability) that appeared reduced in number and size (Fig 5C). Consistent with these results, GlaB strikingly reduced Hh pathway activity as evaluated by the dramatic decrease of the pathway readout Gli1, Gli2 and Ptch1 mRNAs,

stemness markers (Nanog, Oct4) as well as growth (cyclins D1 and D2, PCNA) and oncogenic (NMyc) related signals (Fig 5D). The ability of GlaB to suppress clonogenicity is due to inhibition of stem-like cell proliferation, since BrdU uptake and PCNA protein expression were significantly decreased at early phases (24 and 48 h) of cell expansion (Fig 5E and F). A pro-apoptotic role of GlaB was also observed in MB-SCs, since the percentage of TUNEL-labeled cells and the cleavage of caspase-3 were increased after 48 h of drug treatment (Fig 5G).

In conclusion, the inhibitory activity of GlaB on the subset of both normal and tumor progenitor/stem cells as well as the whole tumor cell populations is restricted to Hh/Gli-dependent cells.

GlaB inhibits Gli-dependent growth of medulloblastoma cells *in vivo*

To study the GlaB effect *in vivo*, we turned to an allograft model of MB cells. Nude mice were grafted with spontaneous primary MB from Ptch1 $^{+/-}$ mice and treated every second day with s.c. injections of GlaB at a concentration of 75 μmol/kg or solvent only (n = 6 for each group).

During an 18-day treatment period, suppression of tumor cell growth was observed in GlaB-treated mice compared to controls (Fig 6A and B). GlaB-treated tumor mass displayed a reduced cellularity where a few MB cells were dispersed in a large amount of Masson's staining-mediated blue-labeled connective tissue, compared to control (Fig 6C). Such a reduced cellularity was caused by inhibition of tumor cell proliferation and survival, since the percentages of Ki67 and TUNEL labeling were decreased and increased, respectively, in GlaB-treated tumors (Fig 6C and D). Consistently, additional markers of cell proliferation (PCNA, cyclins D1 and D2), apoptosis (active caspase-3), oncogenicity (NMyc) and stem-like cell content (Nanog) were also modulated by GlaB, together with a reduction of Gli1 mRNA and protein levels (Fig 6E and F). Overall, these findings suggest that GlaB interferes with several Gli-dependent MB-associated processes.
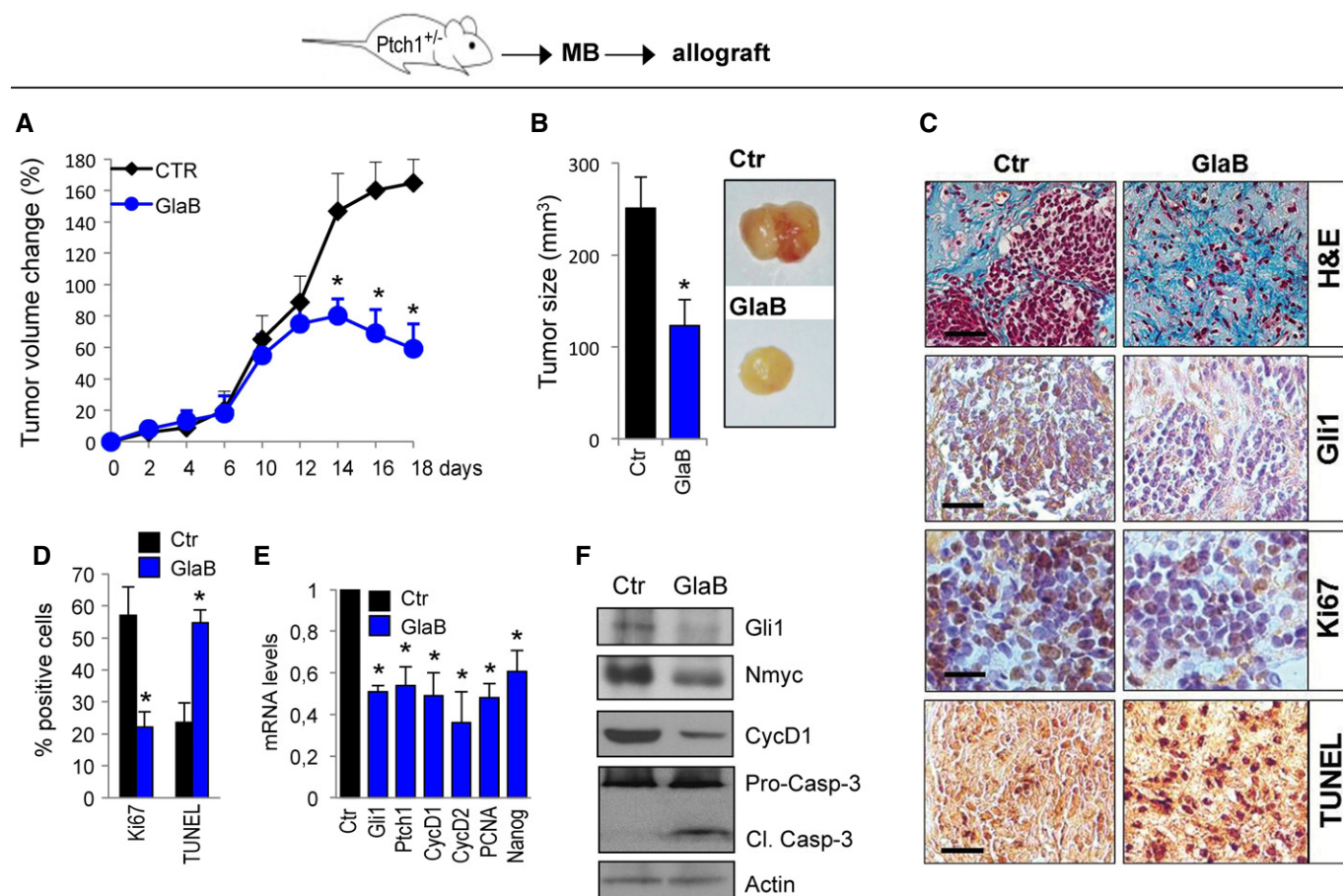

Figure 6. Ptch1 $^{+/-}$ MB allografts.

A   Change of tumor volume during GlaB or vehicle treatment period (18 days).

B   Representative flank allografts average volumes. Error bars indicate SD. *P < 0.05.

C   Representative Masson's trichrome staining of tumors; immunohistochemistry of Gli1, Ki67 and TUNEL stainings. Scale bars represent 35 μm for Masson's trichrome staining, 25 μm for Gli1 and TUNEL, and 10 μm for Ki67 stainings.

D   Quantification of Ki67 and TUNEL stainings from immunohistochemistry shown in (C). Error bars indicate SD. *P < 0.05.

E, F   qRT–PCR and Western blot analysis show Hh and proliferation target mRNA and protein expression levels. For qRT–PCR, results were normalized to endogenous control (β2-microglobulin and *HPRT*). Data show the mean ± SD of tumor (n = 6) for each treatment. *P < 0.05 versus Ctr.

To confirm the inhibitory effect of GlaB to impair MB tumor growth *in vivo*, we used a MB orthotopic xenograft animal model. Human MB Daoy cells were implanted into the cerebellum of NOD/SCID mice. The animals were divided into two groups and treated with GlaB (75 μmol/kg) or solvent alone. After treatment period, mice were sacrificed by *in vivo* perfusion and cerebella were surgically excised. Tumor volume (calculated along serial histologic brain sections as described in Materials and Methods) displayed a significant reduction of the tumor mass formed by Daoy cells in GlaB-treated mice compared to the control (Fig 7A and B). Such a reduced tumor mass was likely caused by inhibition of tumor cell proliferation since the percentages of Ki67 labeling were decreased in GlaB-treated tumors (Fig 7A and C).

GlaB inhibits the growth of Gli-dependent basal cell carcinoma *in vitro* and *in vivo*

In addition to MB, basal cell carcinoma (BCC) is also known as a specific Hh-dependent tumor caused by genetic defects leading to Gli activation (i.e. Ptch1 mutation in Gorlin syndrome). We tested
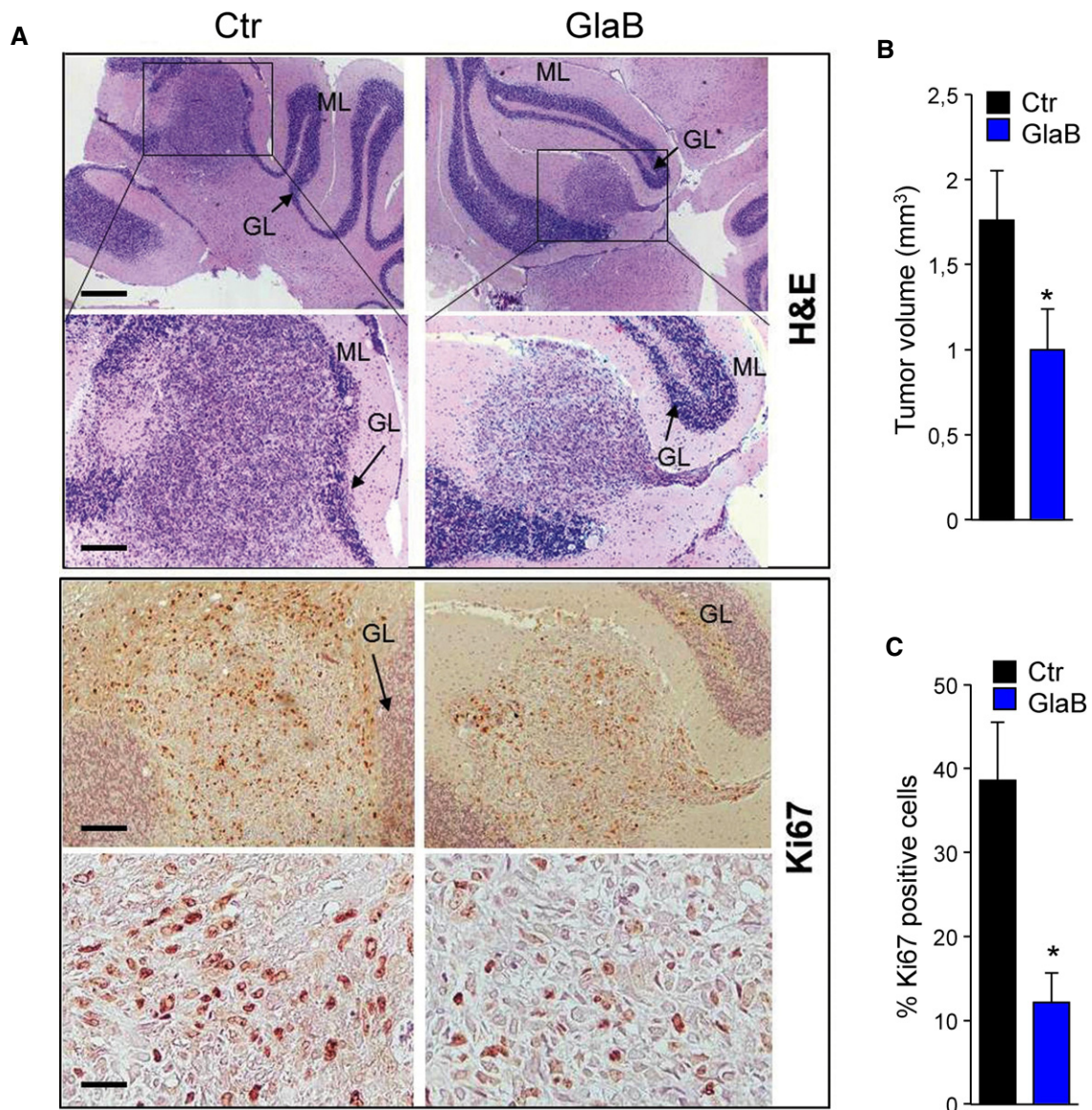

Figure 7. Orthotopic medulloblastoma xenograft models.

A   Representative images (low and high magnification) of H&E (upper panel) and Ki67 immunohistochemical staining (lower panel) of a human Daoy MB cell-derived orthotopic tumor in NOD/SCID mice cerebella after i.p. injections of GlaB. Scale bars represent 500 or 200 μm for H&E staining, and 150 μm or 50 μm for Ki67 staining.

B   Representative tumor average volumes at the end of treatment. Error bars indicate SD. *P* < 0.05.

C   Quantification of Ki67 staining from immunohistochemistry shown in (A). Error bars indicate SD. *P* < 0.05.

the effect of GlaB on ASZ001 BCC cells, previously characterized as an Hh/Gli-dependent tumor cell line harboring Ptch1 deletion (Aszterbaum *et al*, 1999). BCC cell proliferation was impaired by *in vitro* treatment with GlaB together with a suppression of Gli1 mRNA before a drug-induced cell death occurred (Fig 8A–C).

Notably, *in vivo* GlaB-induced tumor growth inhibition was also observed in BCC s.c. allografts. A significant reduction of tumor growth, as well as Gli1 mRNA levels, was observed 18 days after administration of GlaB (100 μmol/kg) compared to solvent alone (Fig 8D, E and H). GlaB-treated BCC allografts also displayed

decreased and increased Ki67 and TUNEL labeling, respectively, as well as strong reduction of Gli1 expression (Fig 8F–H), suggesting a drug-induced impairment of Hh-dependent tumor growth and survival.

Discussion

In this study, we identify the structural requirements of Gli1/DNA functional interaction and exploit this information to discover a
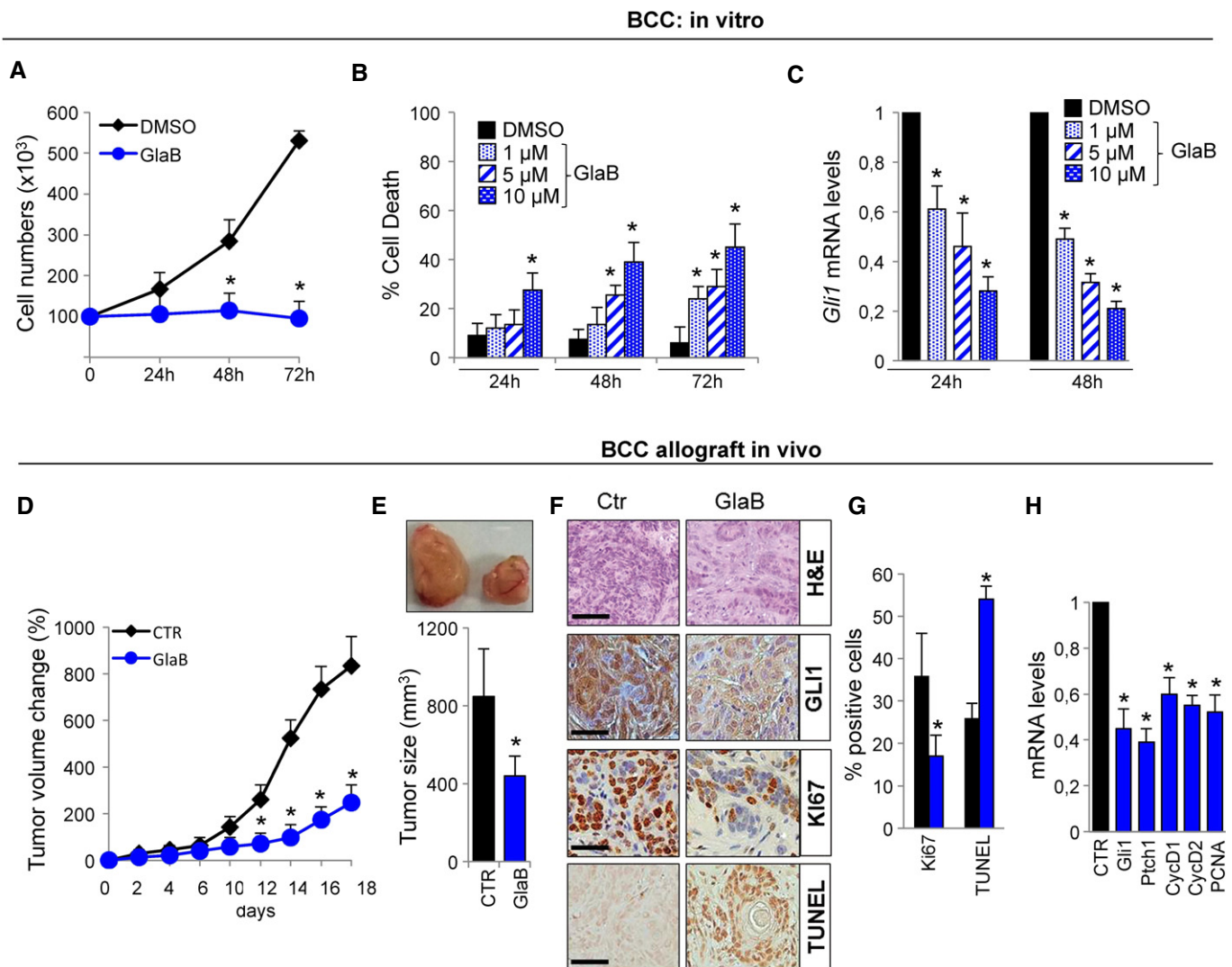

Figure 8.   Inhibition of Gli-dependent BCC tumor cell growth.

A, B   ASZ001 BCC cells were treated with GlaB (5 μM) or DMSO only. After the indicated times, a trypan blue count was performed to determine (A) the growth rate and (B) the percentage of cell death. Data show the mean ± SD of three independent experiments. *$P < 0.05$ versus DMSO.

C   *Gli1* mRNA expression levels were determined by qRT–PCR after treatment of ASZ001 BCC cells with GlaB or DMSO only for the indicated times. Results were normalized to endogenous control (β2-microglobulin and *HPRT*). Data show the mean ± SD of three independent experiments. *$P < 0.05$ versus DMSO.

D–H   GlaB inhibits Gli1-dependent BCC tumor growth in ASZ001 BCC allografts *in vivo*. (D) Change of tumor volume during GlaB or vehicle treatment period (18 days). (E) Representative flank allografts average volumes (upper panel). (F) H&E and immunohistochemical staining of Gli1, Ki67 and TUNEL of allograft tumor samples. Scale bars represent 50 μm for H&E, 25 μm for Gli1, 25 μm for Ki67 and 30 μm for TUNEL stainings. (G) Quantification of Ki67 and TUNEL stainings from immunohistochemistry shown in (F). (H) qRT–PCR of Hh and proliferation target mRNA expression levels. Results were normalized to endogenous control (β2-microglobulin and *HPRT*). Shown is the mean ± SD of tumor (*n* = 6) for each treatment. *$P < 0.05$ versus Ctr.

low-molecular-weight compound capable of inhibiting Hh pathway by targeting Gli1. Such a pharmacologic interference results in an anti-tumor response in cultured cells and *in vivo* in transplanted Hh-dependent tumor mouse models (MB and BCC).

Molecular bases of Gli1/DNA interaction

The structural and functional requirements of Gli1 interaction with target promoters are far to be elucidated, although intensively investigated. We identify here K340 and K350 residues as crucial determinants of Gli1 binding to DNA and of its transcriptional activity. Notably, K350 has been shown by MD to specifically bind to the Gli consensus sequence by means of H-bond interactions with two guanine bases and not by contacting the phosphate backbone, thus providing a likely structural explanation for its critical role in direct targeting specific DNA sequences. Site-specific mutagenesis further supports this model through EMSA and reporter luciferase assays.

   Molecular mechanisms involved in Gli1 and Gli2 function have so far addressed specific residues affected by post-translational modifications occurring outside the DNA binding domain. Phosphorylation of S84 by mTOR/S6K1 releases Gli1 from its inhibitor

SuFu (Wang *et al*, 2012), a mechanism possibly involved also in phosphorylation controlled by RAS/MAPK pathway (reviewed in Aberger & Ruiz I Altaba, 2014). Furthermore, Y859, Y872 and S1060 of Gli1 are cooperatively bound by the E3 ligase Itch (Di Marcotullio *et al*, 2006a, 2011), while D_C degrons (residues 462–467) bind βTrCP, all leading to protein ubiquitination and degradation (Huntzicker *et al*, 2006). Finally, K518 (Gli1) and K757 (Gli2) are instead acetylatable residues preventing transcriptional activity (Canettieri *et al*, 2010; Coni *et al*, 2013b), whereas T374 of the Gli1ZF is a major PKA site contrasting Gli1 localization into the nucleus (Sheng *et al*, 2006). Once phosphorylated by aPKCι/λ, S243 and T304 of the GliZF confer to the protein an enhanced ability to form a complex with DNA (Atwood *et al*, 2013), possibly through a conformational change or binding stabilization or the recruitment of additional co-regulatory proteins, as these amino acids are located in ZF-1 and ZF-3 that mainly establish a few contacts only with the phosphate backbone. Overall, these data also imply that drug-mediated interference with cell signals driving such a post-translational modification may impact on Gli1 function. Instead, neither acetylation nor ubiquitination has been reported to affect K350 and K340, suggesting that these residues are involved per se in DNA recognition. Therefore, they are likely direct druggable targets. To this
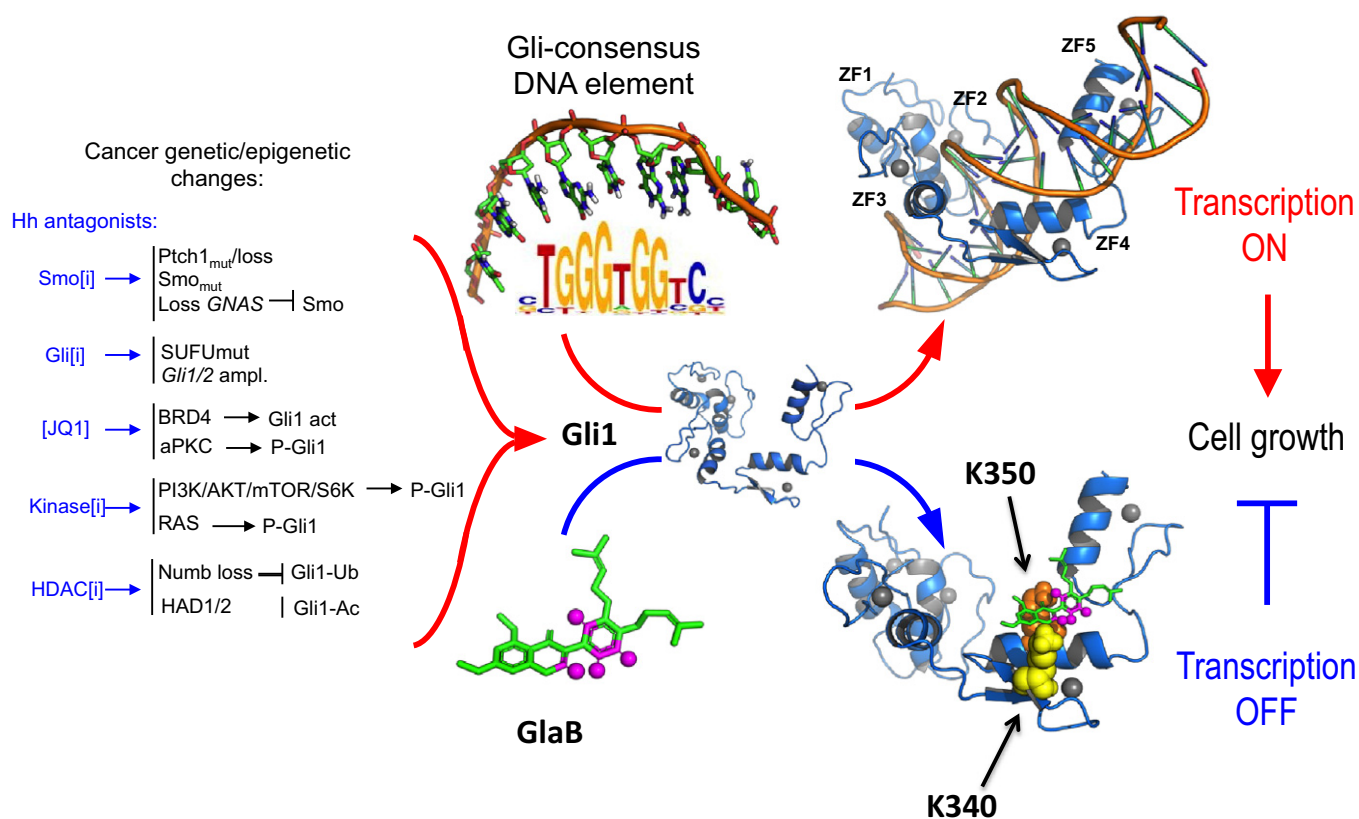

Figure 9. Schematic model of GlaB mechanisms of action.
Several tumors harbor a number of genetic/epigenetic changes that activate Hh signaling to induce the Gli1 transcriptional activity. These mechanisms may be targeted by specific inhibitors (i.e. against Smo, BRD4, kinases, HDAC1/2). Gli1 suppression may be achieved by the common route of the interaction of Gli1 to DNA that is mediated by specific residues such as K350 localized in Gli1 ZF4. GlaB achieves the most profitable interactions on a groove sculpted by K340 residue on the surface of ZF4 as well as a direct binding to K350. In this way, GlaB would mask critical DNA docking sites and impair the Gli1/DNA interaction, thus blunting the expression of Gli1 target genes and repressing cell growth consequently.

regard, by combining mutagenesis studies with NMR spectroscopy and molecular simulations, we demonstrate here that K340 and K350 are also bound by GlaB, the first described small molecule able to impair Hh oncogenic activity *in vitro* and *in vivo* by inhibiting Gli1 interaction to DNA. K340 may sculpt a groove over the side chain of R354 on the rather flat surface of ZF4 where GlaB achieves the most profitable interactions, whereas K350 contacts directly GlaB by H-bond. These findings are consistent with the lack of activity of GlaB on several enzymes that have been described to modulate the function of Gli through post-synthetic modifications (i.e. the phosphokinases Dyrk1, GSK3β, PKA, p70S6K, RAS/ERK). In this way, we suggest that GlaB, binding to specific residues involved in Gli1/DNA interaction, would mask critical DNA docking sites, blunting the expression of target genes (Fig 9).

Translational relevance of regulation of Gli1/DNA interaction by small molecules: Smo/Gli activation redundancy versus the bottleneck of Gli/DNA interference

The biological relevance of our data is provided by the demonstration that Gli1/DNA interaction is druggable in order to inhibit the Gli1 hyperactivation induced not only by upstream Smo/cilium-derived signals, but also by the emerging downstream bypass mechanisms (i.e. Gli1 phosphorylation, gene copy number amplification, BRD4-driven epigenetic activation, deubiquitination, deacetylation or activation by aPKCι/λ or p70S6K or RAS/ERK) that are responsible for the resistance to anti-Smo drugs frequently observed in Hh-dependent tumor initiation, progression and relapse (Amakye *et al*, 2013; Aberger & Ruiz I Altaba, 2014; Tang *et al*, 2014). Indeed, non-canonical Hh/Gli pathway activation independent of Smo signals is emerging as an oncogenic load driven by genetic and/or epigenetic hyperactivation of several oncogenes commonly observed in tumors (Aberger & Ruiz I Altaba, 2014) (Fig 9). The redundancy of such Gli-activating mechanisms observed in several types of Hh-dependent tumors may represent a challenge for the design of targeted personalized therapies. PI3K/AKT inhibitors have been described to rescue the anti-Smo drug resistance through inactivation of S6K1-enhanced Gli1 phosphorylation (Buonamici *et al*, 2010). Similarly, hyperactivation of aPKCι/λ in BCC accounts for the resistance to Smo inhibitor drugs and can be rescued by specific kinase inhibitors (Atwood *et al*, 2013). Finally, HDAC inhibitors are effective in suppressing Hh signaling and tumor growth cancer cell populations where HDAC1/2 are overexpressed (Canettieri *et al*, 2010). Therefore, drug-mediated inhibition of the multiple signals that enhance Gli1 through targeting its post-translational modifications would appear to require a combination of therapeutic approaches (Fig 9).

Instead, the identification of the structural requirements of Gli1/DNA binding and of an interfering small molecule provides valuable insights to optimize the pharmacologic strategies of direct Gli1 targeting to prevent its interaction with DNA and the subsequent functional outputs. This would be an appealing therapeutic strategy focusing on the unique downstream Gli transcriptional effector rather than targeting a variety of upstream oncogenic deregulated signals that either characterize each type of tumor or sustain the evolution of tumor throughout drug sensitivity changes.

Materials and Methods

Electrophoretic mobility shift assay

The canonical Gli binding sequence (Gli-BS, 5′–TTGCCTAC CTGGGTGGTCTCTCCACTT–3′) or its mutant form unable to bind Gli1 (5′–TTGCCTACCTCCCACTTCTCTCCACTT–3′) was produced by annealing complementary oligos. Fragments were end-labeled with γ³²P-ATP using T4 polynucleotide kinase in accordance with manufacturer's instructions and purified through G25 columns (Amersham Pharmacia, Milan, Italy) and used as probe for electrophoretic mobility shift assays (EMSA). Glutathione S-transferase (GST) fusion proteins, only-GST, GST-Gli1ZF-WT (Gli1 zinc finger fragment: aa 242–424), GST-Gli1ZF-K340A or GST-Gli1ZF-K350A, were produced as previously described (De Smaele *et al*, 2008). Binding reactions were performed at room temperature for 20 min using 4 µg of GST fusion proteins and 20,000 c.p.m. of ³²P-end-labeled probes in 20 µl. The final concentration of components of the binding buffer for all EMSA experiments were the following: 50 mM HEPES (pH 7.5), 100 mM KCl, 5 mM DTT, 1 mM EDTA, 20% glycerol, 0.05% NP-40, 0.2 µg/µl BSA, 5 mM MgCl₂ and 50 µg/ml poly(dI)-poly(dC). Competition experiments were performed by adding 50× molar excess of cold oligonucleotides. Complexes were resolved on a non-denaturating 5% PAGE, dried and exposed for autoradiography. Radiolabeled bands were quantitated with a PhosphorImager densitometer (Molecular Dynamics) using IMAGE QUANT software to assess the ratio of probe bound to GliZF versus free probe.

Docking-based analysis of GlaB binding to Gli1 and its alanine mutants

The binding conformation of GlaB to Gli1ZF-WT, Gli1ZF-K340A, Gli1ZF-K350A and Gli1ZF-K340A/K350A was studied by molecular docking simulations, performed with the same program used for virtual screening. Docking efficacy was improved to 200%, while the binding site radius was set at 26 Å. Docking complexes were further relaxed by 5,000 steps of energy minimization in explicit water solvent. GlaB affinity was then estimated by means of the MM-GBSA method, and the pK_d was computed by the empirical functions implemented in XSCORE (Wang *et al*, 2002, 2003).

Molecular dynamics simulations

Initial coordinates of the Gli1ZF/DNA complex were retrieved from the Protein Data Bank, under the PDB accession code 2GLI (X-ray crystal structure at 2.6 Å resolution) (Pavletich & Pabo, 1993). Coordinates of water molecules were removed from the complex, and original cobalt ions were manually replaced with zinc ions within the coordination system of each ZF. The Amber11 program was used for generating MD trajectories and performing energy calculations. AmberTools1.5 was used for preparing input coordinates and topology files, and for performing the preliminary analysis of MD trajectories by the *ptraj* and *cpptraj* modules. The ff99bsc0 force field, which incorporates updates and modifications to the successful ff99 force field, was used. Parameters for the zinc ion and residues within the zinc coordination system were adapted from a previous QM study (Mori *et al*, 2010). The Gli1ZF/DNA complex

was inserted in a cuboid box of explicit TIP3P-typed water molecules, buffering 8 Å from the macromolecular system. The total charge of the system was neutralized by the addition of sodium counterions. The solvated macromolecular system was first energy minimized by using SANDER. In details, water molecules and counterions were first minimized for 250 steps by using a steepest descent algorithm (SD) and for 750 steps by using a conjugate gradient algorithm (CG), while keeping Gli1ZF/DNA frozen. Then, the solvated system was energy minimized for 1,000 steps SD and further 4,000 steps CG without positional restraints, before heating from 0 to 300 K for 50 ps with the Langevin thermostat. Density was equilibrated for 50 ps. In these steps, Gli1 and DNA backbones were restrained with a harmonic force constant of 5.0 kcal/mol/Å^2. Restrained MD trajectories were produced for 3 ns while the force constant was gradually decreased from 5 to 1 kcal/mol/Å^2. Finally, unrestrained MD trajectories were generated for 20 ns. During all MD simulations, a time step of 0.001 ps was used. Four independent replicas of unrestrained MD simulations were performed, starting from slightly different initial coordinates.

In silico alanine scanning

The alanine scanning procedure implemented in Amber11 was used. The calculation of the delta energy of binding (ΔG) of Gli1ZF to DNA was performed along 200 frames of each MD trajectory, by means of the Molecular Mechanics Poisson Boltzmann Surface Area (MM-PBSA) method. The delta–delta energy of binding (ΔΔG) was calculated as the difference between the ΔG of each Gli1ZF alanine mutant and the ΔG of the Gli1ZF-WT. Water molecules closest to R354 and K381 were explicitly accounted for in ΔΔG calculations.

NMR

NMR measurements were performed on a spectrometer operating at 600 MHz for ^{1}H. The temperature was controlled to ± 0.1°C. The spin-lattice selective relaxation rates were measured by using the inversion recovery pulse sequence (180°-τ-90°-t)$_n$ and by applying a selective π-pulse at the selected frequency. Measurements were carried out for some protons of GlaB in the free state and in the presence of different proteins ([GlaB] = 0.412 mM; GlaB/protein = 150:1, DMSO-d_6 solutions, 25°C). Each measurement was repeated at least four times.

Source and characterization of GlaB

Glabrescione B (GlaB) was extracted and purified from seeds of *Derris glabrescens* (Leguminosae) by following the procedure already described (Delle Monache *et al*, 1977). Chemical identity was established by NMR analysis and mass spectrometry. Purity of the sample used in this study was higher than 99.5% by HPLC, performed on a Phenomenex Luna C18, 5.0-μm stainless steel column (250 × 4.0 mm L. × I.D.). Mobile Phase A: H_2O:ACN, 95:5 v/v. Mobile Phase B: H_2O:ACN, 5:95. Gradient elution: 0–5 min A:B, 50:50; 5–20 min up to 100% B; 20–25 min 100% B. Flow rate: 1.0 ml/min. UV detection at 295 nm: retention time: 17.29 min.

GlaB characterization data are described in Supplementary Materials and Methods.

6-day-old mice injections

Six-day-old CD1 mice were randomly divided into two groups (n = 6) and injected s.c. with solvent only (2-hydroxypropyl-β-cyclodextrin:ethanol, 3:1) or GlaB in solvent (100 μmol/kg) for 2 days (2-hydroxypropyl-β-cyclodextrin was purchased from Sigma Aldrich). Cerebella were collected, and mRNA levels were determined by qRT–PCR. Histological sections were stained and surface size calculated by Image Pro Plus 6.2 software.

Allograft experiments

Spontaneous MB from Ptch1$^{+/-}$ mice was isolated, minced and pipetted to obtain a single-cell suspension. Equal volumes of cells (2 × 10^6) were injected s.c. at the posterior flank of female BALB/c nude mice (*nu/nu*) (Charles River Laboratories, Lecco, Italy). Tumors were grown until a median size of ~100 mm^3. Animals were randomly divided into two groups (n = 6) and treated with solvent only (2-hydroxypropyl-β-cyclodextrin:ethanol, 3:1) or GlaB in solvent (75 μmol/kg) for 18 days. 2 × 10^6 ASZ001 BCC cells were resuspended in an equal volume of 154CF medium and Matrigel (BD Biosciences, Heidelberg, Germany) and injected s.c. at the posterior flank of female NOD/SCID mice (Charles River Laboratories, Lecco, Italy), as previously described (Eberl *et al*, 2012). Tumors were grown until a median size of ~200 mm^3. Animals were randomly divided into two groups (n = 6) and treated with solvent only (2-hydroxypropyl-β-cyclodextrin:ethanol, 3:1) or GlaB in solvent (100 μmol/kg) for 18 days. Tumor growth was monitored by measuring the size by caliper. Tumor volumes change was calculated by the formula length × width × 0.5 × (length + width) (Lauth *et al*, 2007). All animal experiments were approved by local ethics authorities.

Intracerebral tumor cell implantation

Adult female NOD/SCID mice were obtained from Charles River Laboratories. Briefly, mice were anesthetized by i.p. injection of ketamine (10 mg/kg) and xylazine (100 mg/kg). The posterior cranial region was shaved and placed in a stereotaxic head frame. Daoy cells (prepared from fresh culture to ensure optimal viability of cells during tumor inoculation) were stereotaxically implanted into the cerebellum (0.2 × 10^6/3 μl) at an infusion rate of 1 μl/min by using the following coordinates according to the atlas of Franklin and Paxinos: 6.6 mm posterior to the bregma; 1 mm lateral to the midline; and 2 mm ventral from the surface of the skull. After injection, the cannula was kept in place for about 5 min for equilibration of pressures within the cranial vault. The skin was closed over the cranioplastic assembly using metallic clips. After 10 days following tumor implantation, the animals were randomly divided into two groups (n = 6) and treated i.p with solvent only (2-hydroxypropyl-β-cyclodextrin:ethanol, 3:1) or GlaB in solvent (75 μmol/kg) every second day. After 25 days of treatment, animals were sacrificed and *in vivo* perfused and brains were fixed in 4% formaldehyde in 0.1 M phosphate buffer (pH 7.2) and paraffin embedded. For brain tumor volume calculation, serial thick coronal sections (2 μm) starting from the mesencephalon to the end of cerebellum were performed. The analysis was performed on 40 sections of 2 μm, sampled every 40 μm on the horizontal plan of the cerebellum, in which the

cerebellum was identified and outlined at 2.5× magnification. Every 40 μm of brain slice H&E staining was performed. Tumor area of every slice was evaluated with a microscope (Axio Imager M1 microscope; Leica Microsystems GmbH, Wetzlar, Germany) equipped with a motorized stage and Image Pro Plus 6.2 software. The following formula was used to calculate brain tumor volume: tumor volume = sum of measured area for each slice × slice thickness × sampling frequency. All animal experiments were approved by local ethics authorities.

Statistical analysis

Statistical analysis was performed using StatView 4.1 software (Abacus Concepts). Statistical differences were analyzed with the Mann–Whitney U-test for nonparametric values, and a $P < 0.05$ was considered significant. Results are expressed as mean $\pm$ SD from an appropriate number of experiments (at least three biological replicas), as indicated in the figure legends.

Supplementary information for this article is available online: http://emboj.embopress.org

Author contributions

PI, MM and RA designed and performed experiments, analyzed data and performed *in silico* studies. BB provided the natural products library. BB, FG, ST and CI isolated, purified and characterized organic molecules, performed analytic studies and analyzed data. FA and GUB performed NMR measurements of proton relaxation rates. MS, AP, EM, DD and DC performed experiments and contributed to stem cells maintenance. GC, EDS, EF, IS and MB helped to interpret data. BB, AG and LDM designed experiments, interpreted data and wrote the manuscript.

Conflict of interest

The authors declare that they have no conflict of interest.

References

Aberger F, Ruiz I Altaba A (2014) Context-dependent signal integration by the GLI code: the oncogenic load, pathways, modifiers and implications for cancer therapy. *Semin Cell Dev Biol* 33: 93–104

Amakye D, Jagani Z, Dorsch M (2013) Unraveling the therapeutic potential of the Hedgehog pathway in cancer. *Nat Med* 19: 1410–1422

Aszterbaum M, Epstein J, Oro A, Douglas V, LeBoit PE, Scott MP, Epstein EH Jr (1999) Ultraviolet and ionizing radiation enhance the growth of BCCs and trichoblastomas in patched heterozygous knockout mice. *Nat Med* 5: 1285–1291

Atwood SX, Li M, Lee A, Tang JY, Oro AE (2013) GLI activation by atypical protein kinase C ι/λ regulates the growth of basal cell carcinomas. *Nature* 494: 484–488

Beauchamp EM, Ringer L, Bulut G, Sajwan KP, Hall MD, Lee YC, Peaceman D, Ozdemirli M, Rodriguez O, Macdonald TJ, Albanese C, Toretsky JA, Uren A (2011) Arsenic trioxide inhibits human cancer cell growth and tumor development in mice by blocking Hedgehog/Gli pathway. *J Clin Invest* 121: 148–160

Berman DM, Karhadkar SS, Hallahan AR, Pritchard JI, Eberhart CG, Watkins DN, Chen JK, Cooper MK, Taipale J, Olson JM, Beachy PA (2002) Medulloblastoma growth inhibition by hedgehog pathway blockade. *Science* 297: 1559–1561

Bosco-Clément G, Zhang F, Chen Z, Zhou HM, Li H, Mikami I, Hirata T, Yagui-Beltran A, Lui N, Do HT, Cheng T, Tseng HH, Choi H, Fang LT, Kim IJ, Yue D, Wang C, Zheng Q, Fujii N, Mann M *et al* (2013) Targeting Gli transcription activation by small molecule suppresses tumor growth. *Oncogene* 33: 2087–2097

Briscoe J, Thèrond PP (2013) The mechanisms of Hedgehog signalling and its roles in development and disease. *Nat Rev Mol Biol* 14: 416–429

Buonamici S, Williams J, Morrissey M, Wang A, Guo R, Vattay A, Hsiao K, Yuan J, Green J, Ospina B, Yu Q, Ostrom L, Fordjour P, Anderson DL, Monahan JE, Kelleher JF, Peukert S, Pan S, Wu X, Maira SM *et al* (2010) Interfering with resistance to smoothened antagonists by inhibition of the PI3K pathway in medulloblastoma. *Sci Transl Med* 2: 51ra70

Canettieri G, Di Marcotullio L, Greco A, Coni S, Antonucci L, Infante P, Pietrosanti L, De Smaele E, Ferretti E, Miele E, Pelloni M, De Simone G, Pedone EM, Gallinari P, Giorgi A, Steinkühler C, Vitagliano L, Pedone C, Schinin ME, Screpanti I *et al* (2010) Histone deacetylase and Cullin3-REN (KCTD11) ubiquitin ligase interplay regulates Hedgehog signalling through Gli acetylation. *Nat Cell Biol* 12: 132–142

Clement V, Sanchez P, de Tribolet N, Radovanovic I, Ruiz I Altaba A (2007) Hedgehog-Gli1 signaling regulates human glioma growth, cancer stem cell self-renewal, and tumorigenicity. *Curr Biol* 17: 165–172

Coni S, Antonucci L, D'Amico D, Di Magno L, Infante P, De Smaele E, Giannini G, Di Marcotullio L, Screpanti I, Gulino A, Canettieri G (2013b) Gli2 acetylation at lysine 757 regulates hedgehog-dependent transcriptional output by preventing its promoter occupancy. *PLoS ONE* 8: e65718

Coni S, Infante P, Gulino A (2013a) Control of stem cells and cancer stem cells by Hedgehog signaling: pharmacologic clues from pathway dissection. *Biochem Pharmacol* 85: 623–628

Dahlén A, Fletcher CD, Mertens F, Fletcher JA, Perez-Atayde AR, Hicks MJ, Debiec-Rychter M, Sciot R, Wejde J, Wedin R, Mandahl N, Panagopoulos I (2004) Activation of the Gli oncogene through fusion with the beta-actin gene (ACTB) in a group of distinctive pericytic neoplasms: pericytoma with t(7;12). *Am J Pathol* 164: 1645–1653

De Smaele E, Fragomeli C, Ferretti E, Pelloni M, Po A, Canettieri G, Coni S, Di Marcotullio L, Greco A, Moretti M, Di Rocco C, Pazzaglia S, Maroder M, Screpanti I, Giannini G, Gulino A (2008) An integrated approach identifies Nhlh1 and Insm1 as Sonic Hedgehog–regulated genes in developing cerebellum and medulloblastoma. *Neoplasia* 10: 89–98

Delle Monache F, Cairo Valeira G, Sialer de Zapata D, Marini-Bettolo GB (1977) 3-Aryl-4-methoxycoumarins and isoflavones from Derris glabrescens. *Gazz Chim Ital* 107: 403–407

Delle Monache F (1985) Chemistry and biological activity of the secondary metabolites of Vismieae. *Rev Latinoamer Quim* 16-1: 5–15

Di Marcotullio L, Ferretti E, De Smaele E, Screpanti I, Gulino A (2006b) Suppressors of Hedgehog signaling: linking aberrant development of neural progenitors and tumorigenesis. *Mol Neurobiol* 34: 193–204

Di Marcotullio L, Ferretti E, Greco A, De Smaele E, Po A, Sico MA, Alimandi M, Giannini G, Maroder M, Screpanti I, Gulino A (2006a) Numb is a suppressor of Hedgehog signalling and targets Gli1 for Itch-dependent ubiquitination. *Nat Cell Biol* 8: 1415–1423

Di Marcotullio L, Greco A, Mazzà D, Canettieri G, Pietrosanti L, Infante P, Coni S, Moretti M, De Smaele E, Ferretti E, Screpanti I, Gulino A (2011) Numb activates the E3 ligase Itch to control Gli1 function through a novel degradation signal. *Oncogene* 30: 65–76

Eberl M, Klingler S, Mangelberger D, Loipetzberger A, Damhofer H, Zoidl K, Schnidar H, Hache H, Bauer HC, Solca F, Hauser-Kronberger C, Ermilov AN, Verhaegen ME, Bichakjian CK, Dlugosz AA, Nietfeld W, Sibilia M, Lehrach H, Wierling C, Aberger F (2012) Hedgehog-EGFR cooperation response genes determine the oncogenic phenotype of basal cell carcinoma and tumour-initiating pancreatic cancer cells. *EMBO Mol Med* 4: 218–233

Galimberti F, Busch AM, Chinyengetere F, Ma T, Sekula D, Memoli VA, Dragnev KH, Liu F, Johnson KC, Guo Y, Freemantle SJ, Andrew AS, Greninger P, Robbins DJ, Settleman J, Benes C, Dmitrovsky E (2012) Response to inhibition of Smoothened in diverse epithelial cancer cells that lack Smoothened or Patched 1 mutations. *Int J Oncol* 41: 1751–1761

Garg N, Po A, Miele E, Campeseq A, Begalli F, Silvano M, Infante P, Capalbo C, De Smaele E, Canettieri G, Di Marcotullio L, Screpanti I, Ferretti E, Gulino A (2013) microRNA-17-92 cluster is a direct Nanog target and controls neural stem cell through Trp53inp1. *EMBO J* 32: 2819–2832

Goodrich L, Milenkovic L, Higgins KM, Scott MP (1997) Altered neural cell fates and medulloblastoma in mouse Patched mutants. *Science* 277: 1109–1113

Gulino A, Di Marcotullio L, Canettieri G, De Smaele E, Screpanti I (2012) Gli control by ubiquitination/acetylation interplay. *Vitam Horm* 88: 211–227

Hahn H, Wojnowski L, Specht K, Kappler R, Calzada-Wack J, Potter D, Zimmer A, Müller U, Samson E, Quintanilla-Martinez L, Zimmer A (2000) Patched target Igf2 is indispensable for the formation of medulloblastoma and rhabdomyosarcoma. *J Biol Chem* 275: 28341–28344

Hatten ME, Roussel MF (2011) Development and cancer of the cerebellum. *Trends Neurosci* 34: 134–142

He X, Zhang L, Chen Y, Remke M, Shih D, Lu F, Wang H, Deng Y, Yu Y, Xia Y, Wu X, Ramaswamy V, Hu T, Wang F, Zhou W, Burns DK, Kim SH, Kool M, Pfister SM, Weinstein LS *et al* (2014) The G protein α subunit Gαs is a tumor suppressor in Sonic hedgehog-driven medulloblastoma. *Nat Med* 20: 1035–1042

Huntzicker EG, Estay IS, Zhen H, Lokteva LA, Jackson PK, Oro AE (2006) Dual degradation signals control Gli protein stability and tumor formation. *Genes Dev* 20: 276–281

Hyman JM, Firestone AJ, Heine VM, Zhao Y, Ocasio CA, Han K, Sun M, Rack PG, Sinha S, Wu JJ, Solow-Cordero DE, Jiang J, Rowitch DH, Chen JK (2009) Small-molecule inhibitors reveal multiple strategies for Hedgehog pathway blockade. *Proc Natl Acad Sci USA* 106: 14132–14137

Jagani Z, Mora-Blanco EL, Sansam CG, McKenna ES, Wilson B, Chen D, Klekota J, Tamayo P, Nguyen PT, Tolstorukov M, Park PJ, Cho YJ, Hsiao K, Buonamici S, Pomeroy SL, Mesirov JP, Ruffner H, Bouwmeester T, Luchansky SJ, Murtie J *et al* (2010) Loss of the tumor suppressor Snf5 leads to aberrant activation of the Hedgehog-Gli pathway. *Nat Med* 16: 1429–1433

Kim J, Lee JJ, Kim J, Gardner D, Beachy PA (2010) Arsenic antagonizes the Hedgehog pathway by preventing ciliary accumulation and reducing stability of the Gli2 transcriptional effector. *Proc Natl Acad Sci USA* 107: 13432–13437

Kinzler KW, Bigner SH, Bigner DD, Trent JM, Law ML, O'Brien SJ, Wong AJ, Vogelstein B (1987) Identification of an amplified, highly expressed gene in a human glioma. *Science* 236: 70–73

Kinzler KW, Vogelstein B (1990) The GLI gene encodes a nuclear protein which binds specific sequences in the human genome. *Mol Cell Biol* 10: 634–642

Kool M, Jones DT, Jäger N, Northcott PA, Pugh TJ, Hovestadt V, Piro RM, Esparza LA, Markant SL, Remke M, Milde T, Bourdeaut F, Ryzhova M, Sturm D, Pfaff E, Stark S, Hutter S, Seker-Cin H, Johann P, Bender S *et al* (2014) Genome sequencing of Shh medulloblastoma predicts genotype-related response to smoothened inhibition. *Cancer Cell* 25: 393–405

Laner-Plamberger S, Kaser A, Paulischta M, Hauser-Kronberger C, Eichberger T, Frischauf AM (2009) Cooperation between GLI and JUN enhances transcription of JUN and selected GLI target genes. *Oncogene* 28: 1639–1651

Lauth M, Bergström A, Shimokawa T, Toftgård R (2007) Inhibition of Gli-mediated transcription and tumor cell growth by small-molecule antagonists. *Proc Natl Acad Sci USA* 104: 8455–8460

Malatesta M, Steinhauer C, Mohammad F, Pandey DP, Squatrito M, Helin K (2013) Histone acetyltransferase PCAF is required for Hedgehog-Gli-dependent transcription and cancer cell proliferation. *Cancer Res* 73: 6323–6333

Manoranjan B, Venugopal C, McFarlane N, Doble BW, Dunn SE, Scheinemann K, Singh SK (2013) Medulloblastoma stem cells: modeling tumor heterogeneity. *Cancer Lett* 338: 23–31

Mas C, Ruiz I Altaba A (2010) Small molecule modulation of HH-Gli signaling: current leads, trials and tribulations. *Biochem Pharmacol* 80: 712–723

Mazzà D, Infante P, Colicchia V, Greco A, Alfonsi R, Siler M, Antonucci L, Po A, De Smaele E, Ferretti E, Capalbo C, Bellavia D, Canettieri G, Giannini G, Screpanti I, Gulino A, Di Marcotullio L (2013) PCAF ubiquitin ligase activity inhibits Hedgehog/Gli1 signaling in p53-dependent response to genotoxic stress. *Cell Death Differ* 20: 1688–1697

Mori M, Dietrich U, Manetti F, Botta M (2010) Molecular dynamics and DFT study on HIV-1 nucleocapsid protein-7 in complex with viral genome. *J Chem Inf Model* 50: 638–650

Mori M, Manetti F, Botta M (2011) Predicting the binding mode of known NCp7 inhibitors to facilitate the design of novel modulators. *J Chem Inf Model* 51: 446–454

Neuhaus D, Williamson M (1989) *The Nuclear Overhauser Effect in Structural and Conformational Analysis*. New York, NY, USA: VCH Publisher

Northcott PA, Jones DT, Kool M, Robinson GW, Gilbertson RJ, Cho YJ, Pomeroy SL, Korshunov A, Lichter P, Taylor MD, Pfister SM (2012) Medulloblastomics: the end of the beginning. *Nat Rev Cancer* 12: 818–834

Pavletich NP, Pabo CO (1993) Crystal structure of a five-finger Gli-DNA complex: new perspectives on zinc fingers. *Science* 261: 1701–1707

Po A, Ferretti E, Miele E, De Smaele E, Paganelli A, Canettieri G, Coni S, Di Marcotullio L, Biffoni M, Massimi L, Di Rocco C, Screpanti I, Gulino A (2010) Hedgehog controls neural stem cells through p53-independent regulation of Nanog. *EMBO J* 29: 2646–2658

Roussel MF, Robinson GW (2013) Role of MYC in Medulloblastoma. *Cold Spring Harb Perspect Med* 3: a014308

Sasai K, Romer JT, Lee Y, Finkelstein D, Fuller C, McKinnon PJ, Curran T (2006) Shh pathway activity is down-regulated in cultured medulloblastoma cells: implications for preclinical studies. *Cancer Res* 66: 4215–4222

Schnidar H, Eberl M, Klingler S, Mangelberger D, Kasper M, Hauser-Kronberger C, Regl G, Kroismayr R, Moriggl R, Sibilia M, Aberger F (2009) Epidermal growth factor receptor signaling synergizes with Hedgehog/GLI in oncogenic transformation via activation of the MEK/ERK/JUN pathway. *Cancer Res* 69: 1284–1292

Schuller U, Heine VM, Mao J, Kho AT, Dillon AK, Han YG, Huillard E, Sun T, Ligon AH, Qian Y, Ma Q, Alvarez-Buylla A, McMahon AP, Rowitch DH, Ligon KL (2008) Acquisition of granule neuron precursor identity is a

critical determinant of progenitor cell competence to form Shh-induced medulloblastoma. *Cancer Cell* 14: 123−134

Sheng T, Chi S, Zhang X, Xie J (2006) Regulation of Gli1 localization by the cAMP/protein kinase A signaling axis through a site near the nuclear localization signal. *J Biol Chem* 281: 9−12

Svard J, Heby-Henricson K, Persson-Lek M, Rozell B, Lauth M, Bergström A, Ericson J, Toftgård R, Teglund S (2006) Genetic elimination of suppressor of Fused reveals an essential repressor function in the mammalian Hedgehog signaling pathway. *Dev Cell* 10: 187−197

Tang Y, Gholamin S, Schubert S, Willardson MI, Lee A, Bandopadhayay P, Bergthold G, Masoud S, Nguyen B, Vue N, Balansay B, Yu F, Oh S, Woo P, Chen S, Ponnuswami A, Monje M, Atwood SX, Whitson RJ, Mitra S *et al* (2014) Epigenetic targeting of Hedgehog pathway transcriptional output through BET bromodomain inhibition. *Nat Med* 20: 732−740

Taylor MD, Liu L, Raffel C, Hui CC, Mainprize TG, Zhang X, Agatep R, Chiappa S, Gao L, Lowrance A, Hao A, Goldstein AM, Stavrou T, Scherer SW, Dura WT, Wainwright B, Squire JA, Rutka JT, Hogg D (2002) Mutations in SuFu predispose to medulloblastoma. *Nat Genet* 31: 306−310

Triscott J, Lee C, Foster C, Manoranjan B, Pambid MR, Berns R, Fotovati A, Venugopal C, O'Halloran K, Narendran A, Hawkins C, Ramaswamy V, Bouffet E, Taylor MD, Singhal A, Hukin J, Rassekh R, Yip S, Northcott P, Singh SK *et al* (2013) Personalizing the treatment of pediatric medulloblastoma: polo-like kinase 1 as a molecular target in high-risk children. *Cancer Res* 73: 6734−6744

Valensin G, Sabatini G, Tiezzi E (1986) Advanced Magnetic resonance techniques in systems of high molecular complexity. 69−76

Verdonk ML, Cole JC, Hartshorn MJ, Murray CW, Taylor RD (2003) Improved protein-ligand docking using GOLD. *Proteins* 52: 609−623

Wang R, Lai L, Wang S (2002) Further development and validation of empirical scoring functions for structure-based binding affinity prediction. *J Comput Aided Mol Des* 16: 11−26

Wang R, Lu Y, Wang S (2003) Comparative evaluation of 11 scoring functions for molecular docking. *J Med Chem* 46: 2287−2303

Wang Y, Ding Q, Yen CJ, Xia W, Izzo JG, Lang JY, Li CW, Hsu JL, Miller SA, Wang X, Lee DF, Hsu JM, Huo L, Labaff AM, Liu D, Huang TH, Lai CC, Tsai FJ, Chang WC, Chen CH *et al* (2012) The crosstalk of mTOR/S6K1 and Hedgehog pathways. *Cancer Cell* 21: 374−387

Wechsler-Reya R, Scott MP (2001) The developmental biology of brain tumors. *Annu Rev Neurosci* 24: 385−428

Yang ZJ, Ellis T, Markant SL, Read TA, Kessler JD, Bourboulas M, Schuller U, Machold R, Fishell G, Rowitch DH, Wainwright BJ, Wechsler-Reya RJ (2008) Medulloblastoma can be initiated by deletion of Patched in lineage-restricted progenitors or stem cells. *Cancer Cell* 14: 135−145

Yauch R, Gerrit L, Dijkgraaf JP, de Sauvage FJ (2009) Smoothened mutation confers resistance to a Hedgehog pathway inhibitor in medulloblastoma. *Science* 326: 572−574

Yoon JW, Liu CZ, Yang JT, Swart R, Iannaccone P, Walterhouse D (1998) GLI activates transcription through a herpes simplex viral protein 16-like activation domain. *J Biol Chem* 273: 3496−3501

Zhan X, Shi X, Zhang Z, Chen Y, Wu JI (2011) Dual role of Brg chromatin remodeling factor in sonic Hedgehog signaling during neural development. *Proc Natl Acad Sci USA* 108: 12758−12763